Accepted Manuscript

Functional Ct Imaging For Identification Of The Spatial Determinants Of Small Airways Disease In Adult Asthma

Alex J. Bell, MMath, Brody H. Foy, BMath, Dr. Matthew Richardson, PhD, Amisha Singapuri, BSc, Dr. Evgeny Mirkes, PhD, Dr. Maarten van den Berge, PhD, David Kay, PhD, Prof., Chris Brightling, FRCP, PhD, Prof., Alexander N. Gorban, PhD, Prof., Craig J. Galbán, PhD, Prof., Salman Siddiqui, MRCP, PhD., Prof.

PII: S0091-6749(19)30087-9

DOI: https://doi.org/10.1016/j.jaci.2019.01.014

Reference: YMAI 13850

To appear in: *Journal of Allergy and Clinical Immunology*

Received Date: 12 April 2018

Revised Date: 9 January 2019

Accepted Date: 14 January 2019

Please cite this article as: Bell AJ, Foy BH, Richardson M, Singapuri A, Mirkes E, van den Berge M, Kay D, Brightling C, Gorban AN, Galbán CJ, Siddiqui S, Functional Ct Imaging For Identification Of The Spatial Determinants Of Small Airways Disease In Adult Asthma, *Journal of Allergy and Clinical Immunology* (2019), doi: https://doi.org/10.1016/j.jaci.2019.01.014.

FUNCTIONAL CT IMAGING FOR IDENTIFICATION OF THE SPATIAL DETERMINANTS OF SMALL AIRWAYS DISEASE IN ADULT ASTHMA

Alex J. Bell, MMath,[a] Brody H. Foy, BMath,[b] Dr. Matthew Richardson, PhD,[a] Amisha Singapuri, BSc,[a] Dr. Evgeny Mirkes PhD,[c] Dr. Maarten van den Berge, PhD, [d] Prof. David Kay, PhD, [b] Prof. Chris Brightling, FRCP, PhD, [a] Prof. Alexander N. Gorban, PhD,[c] Prof. Craig J. Galbán, PhD,[e] Prof. Salman Siddiqui, MRCP, PhD.[a]

[a]NIHR Respiratory Biomedical Research Centre (BRC), Department of Infection, Immunity and Inflammation, University of Leicester, Leicester, UK. [b]Computational Biology, Department of Computer Science, University of Oxford, Oxford, United Kingdom. [c]Department of Mathematics, University of Leicester, Leicester, UK. [d]Department of Pulmonology, University Medical Centre Groningen, Groningen, Netherlands. [e]Department of Radiology, University of Michigan, Michigan, USA.

Corresponding author

Professor Salman Siddiqui, MRCP, PhD

NIHR Biomedical Research Centre (Respiratory Theme)

Respiratory BRU Building

Glenfield Hospital

Groby Road, Leicester, LE3 9QP, UK

Telephone: +44-116-250-2873

Fax: 0116-250-2787

E-mail: ss338@leicester.ac.uk

Declaration of all sources of funding: The current project was funded by the Sir Jules Thorn trust, 'Systems Medicine: Novel Mathematical Approaches to Personalised Care in Asthma Patients' via a clinical senior lecturer award (Professor Siddiqui). Additional funding was received for the original CT scan and physiological analyses from Roche Pharmaceuticals (Professors Brightling and Siddiqui) and the European Union Airways Disease Predicting Outcomes in Patient Specific Computational Models (AirPROM-FP7) consortium. This paper was also supported by the National Institute for Health Research (NIHR) Leicester Respiratory Biomedical Research Centre (BRC), the views expressed are those of the author(s) and not necessarily those of the NHS, the NIHR or the Department of Health.

Conflict of interest statement: Mr. Bell has nothing to disclose. Mr. Foy reports grants from Rhodes Trust, non-financial support from AirPROM-FP7 grant during the conduct of the study. Dr. Richardson has nothing to disclose. Mrs. Singapuri has nothing to disclose. Dr. Mirkes has nothing to disclose. Dr. Berge has nothing to disclose. Prof. Kay has nothing to disclose. Prof. Brightling reports grants from NIHR BRC, grants from EU FP7, during the conduct of the study; grants and personal fees from GSK, grants and personal fees from AZ, grants and personal fees from MedImmune, grants and personal fees from BI, grants and personal fees from Roche/Genentech, grants and personal fees from Novartis, grants and personal fees from Chiesi, grants and personal fees from Mologic, personal fees from PreP, personal fees from 4DPharma, personal fees from TEVA, personal fees from Gilead, personal fees from Glenmark, outside the

submitted work. Prof. Gorban has nothing to disclose. Prof. Galbán has nothing to disclose. Prof. Siddiqui reports grants from NIHR Biomedical Research Centre Grant, grants from Sir Jules Thorne Trust, clinical senior lecturer award (Professor Siddiqui), grants from EU-FP7 AirPROM grant, during the conduct of the study; other from Astra Zeneca, GSK, Owlstone, Mundipharma, Boehringer Ingelheim, personal fees from European Respiratory Society, outside the submitted work.

WORD COUNT: 3,361

ABSTRACT

BACKGROUND: Asthma is a disease characterised by ventilation heterogeneity (VH). A number of studies have demonstrated that VH markers derived using impulse oscillometry (IOS) or multiple breath washout (MBW) are associated with key asthma patient related outcome measures and airways hyper responsiveness. However the topographical mechanisms of VH in the lung remain poorly understood.

OBJECTIVES: We hypothesised that specific regionalisation of topographical small airway disease would best account for IOS and MBW measured indices in patients.

METHODS: We evaluated paired expiratory/inspiratory computed tomography in a cohort of asthmatic (n=41) and healthy volunteers (n=11) to understand the determinants of clinical VH indices commonly reported using IOS and MBW. Parametric response mapping (PRM) was utilised to calculate functional small airways disease marker PRM^{fSAD} and Hounsfield unit (HU) based density change from total lung capacity to functional residual capacity (ΔHU); gradients of ΔHU, in gravitationally perpendicular (parallel), inferior-superior (anterior-posterior) axes, were quantified.

RESULTS: ΔHU gradient in the inferior-superior axis provided the highest level of discrimination of both S_{acin} and R5-20. Patients with a high inferior-superior ΔHU gradient demonstrated evidence of reduced specific ventilation in the lower lobes of the lungs and high levels of PRM^{fSAD}. A computational small airway tree model confirmed that constriction of gravitationally dependant lower zone small airway branches would promote the largest increases

in R5-R20. Ventilation gradients correlated with asthma control and quality of life but not with exacerbation frequency.

CONCLUSIONS: Lower lobe predominant small airways disease is a major driver of clinically measured VH in adult asthma.

WORD COUNT: 248

CLINICAL IMPLICATION

Asthmatics with abnormal small airways ventilation heterogeneity measurements demonstrated small airways disease and reduced ventilation in the inferior regions of the lung, which may impact the effectiveness of inhaled therapies.

CAPSULE SUMMARY

This study analyses spatially localised ventilation heterogeneity in adult asthma using CT imaging and modelling, and presents evidence of inferior to superior ventilation gradient reversal in the disease pathogenesis.

KEY WORDS

Asthma, Computed tomography, Parametric Response Mapping, Imaging, Visualisation, Small airway physiology, Biomarker,

ABBREVIATIONS

LCI: Lung Clearance Index

FRC: Functional Residual Capacity

TLC: Total Lung Capacity

HU: Hounsfield Unit

eHU: HU at expiration state (FRC)

iHU: HU at inspiration state (TLC)

ΔHU: eHU – iHU (regional density change between FRC and TLC)

MBW: Multiple Breath Washout

IOS: Impulse Oscillometry

SAA: Stratified Axial Analysis

VH: Ventilation Heterogeneity

S_{acin}: Acinar VH, measured using phase three slope analysis of multiple breath washout data

SF6: Sulphur hexafluoride

R5-R20: Resistance at 5 Hz minus resistance at 20Hz measured, measured using impulse oscillometry

LDA: Linear Discriminant Function Analysis

PCA: Principal Components Analysis

PRM: Parametric Response Mapping

fSAD: Functional Small Airways Disease

GINA: Global Initiative for Asthma

DICOM: Digital Imaging and Communications in Medicine

INTRODUCTION

Asthma is characterised by spatial heterogeneity in disease and consequent heterogeneity in airways function and lung ventilation [1, 2]. Ventilation heterogeneity (VH) may be captured using imaging approaches that can quantify and regionalise lung ventilation, such as hyper polarised 3-Helium/129-Xenon magnetic resonance imaging (MRI), Oxygen enhanced MR and single photon emission computed tomography (SPECT-CT) [3-7]. Additionally VH can be measured clinically in patients using physiological tidal breathing techniques that measure heterogeneities in lung ventilation (captured using multiple breath washout (MBW) [8, 9]) and mechanical behaviour (captured using impulse oscillometry (IOS) [10]). International guidelines for quality control and assurance of tidal breathing markers of VH derived from IOS and MBW have been proposed [12, 13], supporting their potential role as tools to study early airways disease.

We have previously identified that two specific markers of VH, R5-R20 and S_{acin}, derived from IOS and MBW respectively, are associated with impaired asthma control, quality of life and exacerbations [9, 11]. These observations have been replicated by other groups in parallel studies of adult asthma [14, 15]. Additionally we have previously demonstrated, using computational small airway models and diffusion MRI, that IOS derived R5-R20 and MBW derived Sacin values, are anatomically grounded measures of small and acinar airway anatomical disease respectively, in adult asthmatics [9].

Heterogeneity of ventilation within the lungs is likely to be influenced by both gravitational effects and airway branching, as well as other factors that affect regional lung compliance

(reviewed in [16]). However little is known about the spatial lung determinants of clinical measurements of VH derived using MBW and IOS. This is important as imaging tools are costly, difficult to implement in clinical trials and standardise across centres; physiological tools, if appropriately validated, could serve as simple surrogates of disease heterogeneity captured by sensitive imaging techniques.

Computed tomography (CT) of the lungs has been exploited widely to study lung structure and function relationships in asthma [17, 18]. More recently image registration applied to inspiratory and expiratory CT imaging has been utilised to derive indices of functional small airways disease [19-22]. One specific and widely deployed approach is parametric response mapping (PRM) [20-22]. The PRM approach offers the potential to characterise spatial deformation of a voxel between different acquired CT lung volumes, e.g. functional residual capacity (FRC) and total lung capacity (TLC), over the entire lung, and hence the potential to identify spatial mechanisms of commonly measured MBW and IOS VH markers.

The purpose of this study was to use a range of global and regional airway density change (from functional residual capacity to total lung capacity) imaging biomarkers to understand how spatial variations in VH may contribute to widely reported clinical measurements of VH and small airways disease, captured by IOS and MBW in adult asthma.

Specifically we hypothesised that abnormal regional variations in ΔHU would be a major contributor to abnormal IOS and MBW physiological indices of VH in the small airways and sought to test this hypothesis using a functional CT imaging and computational simulation study.

METHODS

(i) SUBJECTS

The total population for this study consisted of 52 subjects, 41 adult asthmatic and 11 healthy controls. Asthmatic subjects were recruited from Glenfield Hospital in Leicester, UK. Asthma was defined by a clinician diagnosis with one or more of the following objective criterion (i) bronchodilator reversibility of FEV_1 to 400 mcg inhaled salbutamol of $\geq$ 12 % and 200 mls (17 of 41 asthmatics), (ii) Methacholine $PC_{20} \leq 16$ mg /ml (11 of 41 asthmatics) or (iii) peak flow variation of $\geq$ 20% over a 2 week period (13/41).

Asthma severity was classified according to the current Global Initiative for Asthma (GINA) treatment steps [23]. Severe asthmatics within the cohort had similar lung function (post bronchodilator FEV_1/FVC) to previously reported severe asthma cohorts in Leicester, UK [24], but higher average post bronchodilator FEV_1% predicted values.
Aged matched healthy volunteers were recruited via local advertising and staff with normal airway physiology and no features of respiratory disease. All subjects with asthma had been free from exacerbations for at least 6 weeks prior to study entry.

All subjects (asthmatic and healthy volunteers) were non-current smokers, however due to the known association of smoking and small airways disease, pack year smoking exposure was not an exclusion criterion. Only 3/41 patients with asthma had a smoking history of more than 15 pack years.

190

191 *(ii) ETHICAL APPROVAL*

192 The study protocol was approved by the National Research Ethics Committee – East Midlands
193 Leicester (approval number 08/H0406/189), and all subjects gave their written informed consent.

194

195 *(iii) VISITS*

196 Clinical and physiological assessment was performed in the following sequence and over 1-2
197 study visits, no more than 1 week apart. Asthma control was characterised using the modified 6
198 item Juniper Asthma Control Questionnaire (ACQ-6) [25] and Asthma quality of life using the
199 standard 32 question Juniper Asthma Quality of Life Questionnaire (AQLQ) [26]. Exacerbations
200 were defined according to ATS/ERS consensus criteria [27]; a moderate-severe exacerbation is
201 defined as one or more of the following: (i) worsening of asthma that requires use of systemic
202 steroids or an increase in systemic steroids (for patients already receiving maintenance oral
203 steroids) for 3 or more days, or (ii) an admission to hospital or an emergency department
204 requiring systemic steroids.

205 *(iv) LUNG FUNCTION MEASUREMENTS*

206 All lung function tests were performed following the administration of 400 mcg of inhaled
207 salbutamol. Spirometry was performed according to ATS/ERS standards [28].

208

209 Impulse oscillometry (IOS) was performed in triplicate as previously reported and in accordance
210 with international guidelines [12, 13]. Multiple breath washout (MBW) was performed according

to current guidelines [13] by using the sulphur hexafluoride (SF_6) wash-in method as previously described [11]. SF_6 was chosen as the inert tracer gas because of its heavy molar mass and based on previous simulation data from Dutrieue *et al* [29] suggesting that phase III slope sensitivity to SF_6 is maximal at the level of the alveolar duct. Lung clearance indices, S_{cond}, and S_{acin}, were calculated by using custom software written with TestPoint (Measurement Computing Corp, Norton, Mass) as previously described [9, 11]. Body Plethysmography was performed with a constant volume plethysmograph, according to the ATS/ERS recommendation [30]. A minimum of three acceptable tests were performed and the test ended when the repeatability criteria was achieved (FRC within 10% between highest and lowest value). Carbon monoxide uptake in the lung was determined using the single-breath method, according to standard guidelines [31]. Alveolar volume (V_A) and the carbon monoxide transfer coefficient (K_{CO}) were calculated,

(vi) CT IMAGING AND IMAGE ANALYSIS

Volumetric whole-lung scans were obtained following the administration of 400 mcg of inhaled Salbutamol at FRC and TLC in patients lying supine. CT images were quantified using a panel imaging biomarkers (**TABLE E1,** online supplement).

PRM was performed automatically using Imbio's Lung Density Analysis (LDA™) software application (Imbio, LLC, Minneapolis, MN) for all CT data, with registrations performed from TLC to FRC, on segmented voxel sets excluding the major airways (up to 3-4 generations from the trachea). Details on the PRM analysis have been previously reported [19-22]. Relative lung volumes of normal parenchyma (PRM^{Norm}), fSAD (PRM^{fSAD}), emphysema (PRM^{Emph}) and unclassified PRM^{Uncl} were calculated by normalising the sum of all like-classed voxels by the

total lung volume. Additionally features of the PRM joint density histogram (ellipse area, minor axis, major axis and angle to horizontal) were derived in MATLAB 2015a (MATLAB Release 2015a, The MathWorks, Inc., Natick, Massachusetts, United States) [**FIGURE 1A**].

A novel algorithm for evaluating regional density change gradients in a given direction, termed stratified axial analysis (SAA), was developed from per voxel TLC to FRC density change (ΔHU, see **FIGURES E1-E2A**). This allowed us to investigate how ventilation, approximated by ΔHU, varied with respect to axes of interest; particularly the anterior-posterior (approximately parallel to gravity) and inferior-superior (approximately perpendicular to gravity). See **FIGURE 2C and 2D**. Straight line fitting by ordinary least squares criterion was applied to produce $\text{std}(\Delta\text{HU})^{\mathbf{AP}}$, $\overline{\Delta\text{HU}}^{\mathbf{AP}}$, $\text{std}(\Delta\text{HU})^{\mathbf{IS}}$ and $\overline{\Delta\text{HU}}^{\mathbf{IS}}$ as the gradients of fitted lines to SAA derived intervals [**FIGURE E1**], where superscript AP (IS) refers to axis used, anterior-to-posterior (inferior-to-superior); std refers to standard deviation, and $\bar{x}$ refers to **arithmetic mean** of x. $\overline{\Delta\text{HU}}^{\mathbf{IS*}}$ was calculated as the mean of $\overline{\Delta\text{HU}}$ values across every decile, equivalent to scaled (1/9) difference of extreme interval averages, in the inferior-superior direction. N.B. Additional markers classifying lung size asymmetry were also derived using custom scripts in MATLAB [**FIGURE E2B**].

(vii) COMPUTATIONAL SIMULATIONS OF REGIONALISED BRONCHOCONSTRICTION

A detailed outline of the computational models is provided in the online supplement (see section **M3.0** in methods). Briefly, a computational model of airway impedance was designed, based on previous models in the literature to provide simulations of IOS derived R5-R20. In short, a 1D wave equation was used to estimate the impedance of each branch [32], with total impedance

being calculated through summation of parallel and series contributions [33]. Each terminal bronchiole was subtended by a constant-phase viscoelastic model parameterised using data from the literature [34]. The models were adjusted for potential confounding upper airway shunting [35-36].

Simulations of total lung resistance over the frequency range (1-25Hz) were performed on the healthy conducting airway tree created through a combination of CT segmentation (to an average generation of 6), and algorithmic generation (to an average generation of 16) as previously reported [37]. For each simulation, constrictions were applied to either the lowest or highest 25% of small airways (≤ 2mm in diameter), relative to the supine or orthostatic position, to simulate the effects of gravitationally dependant airways. The constriction rates (the percentage an airway radius was reduced by, denoted c) were drawn uniformly from the range (0-70%), and applied homogeneously, using the same c for all airways, or heterogeneously, drawing each constriction from the normal distribution with mean c, and standard deviation 0.2c. For each simulation the output R5-R20 was calculated.

STATISTICAL ANALYSIS

Statistical analyses were performed in MATLAB 2015a. Kolmogorov-Smirnov tests were applied to check likelihood of a normal distribution. Binary group comparisons were performed using two-sample t-test (parametric data) and Mann-Whitney U-test (non-parametric data); for multiple group comparisons one-way ANOVA test was utilised (parametric data) and Kruskal-Wallis test (non-parametric data). Multiple-comparison procedures were performed with Tukey's honest significant difference criterion. Subgroups were determined by GINA treatment steps, and

according to mean S_{acin} and R5-R20. 16 subjects (roughly one third of total population) at each end of R5-R20 and S_{acin} distributions were utilised in tertile polar analysis, at SAA inferior-superior deciles, where statistical significance was determined using two-sided Wilcoxon Rank-Sum test.

Average Pearson's correlation co-efficient ($\bar{r}$) is reported for simple linear correlations. CT biomarkers sets were defined using Kaiser-Rule determined principal components analysis (PCA) and utilised for linear regression analyses to evaluate correlation with clinical traits and physiology. Linear discriminant analysis (LDA) was applied to determine class separation of VH markers S_{acin} and R5-R20 using combinations of CT imaging features, clinical features and spirometry. Negative binomial regression was used to evaluate the relationship between exacerbations and imaging biomarkers and Pearson correlations for association between asthma control/quality of life and imaging ventilation gradient biomarkers.

A p-value of $p < 0.05$ was utilised to define statistically significant results in all tests.

RESULTS

Clinical characteristics of the population are outlined in **TABLE 1**. Asthmatic patients were matched for age and sex to healthy volunteers. The asthmatics population had significantly greater eosinophilic airway inflammation and physiological evidence of airways dysfunction and VH when compared to healthy volunteers. There were no significant differences in VH markers R5-R20 and S_{acin} across GINA treatment intensity groups. Of the 3/41 asthmatic patients with a smoking history of more than 15 pack years, all had a PRM emphysema (PRM^{Emph}) score that was less than the mean + 1.96 SD [5% PRM^{Emph}] in a healthy aged matched population of 98 subjects [38] and preserved KCO % predicted values [**TABLE 1**].The three patients all had evidence of asthma objectively (one had 78% FEV_1 reversibility, one had a PC_{20} methacholine of 2 mg/ml, one had 49% FEV_1 reversibility). Furthermore of these three patients only 2 patients demonstrated a post BD FEV_1/FVC < lower limit of normal (LLN) (63% predicted in both patient respectively with a post BD FEV_1% of 72% and 57% respectively).

Imaging biomarkers of global lung VH are not associated with small airway VH markers R5-R20 and S_{acin}.

TABLE E1 in the online supplement outlines the formal definition of all of the CT scan derived imaging biomarkers. **TABLE E2** in the online supplement presents comparisons of the global and regional imaging biomarkers comparing asthmatic and healthy cases =across the spectrum of GINA treatment intensity.

Asthmatic cases demonstrated significantly smaller PRM ellipse major diameters and smaller ellipse angles and had narrower distributions (standard deviations) of voxel HU change from

FRC-TLC ($p<0.05$) when compared to controls – indicative of less overall VH.

Asthmatics did not differ from controls with respect to standard PRM markers (PRM^{Norm}, PRM^{fSAD} and PRM^{Emph}) [**TABLE E2**]. In contrast patients who demonstrated FEV_1/FVC (%) less than the median population value (primarily asthmatics) had higher levels of PRM^{fSAD} and smaller PRM global ellipse areas (suggestive of less global heterogeneity) when compared to patients with FEV_1/FVC(%) ≥ than the median value ($p<0.05$). [**FIGURE 1 B-C**]. These observations were not replicated with the small airway indices of VH R5-R20 and S_{acin} [**FIGURE E3**] and indicate that global PRM indices in the lung track with spirometry defined airflow obstruction in contrast to small airway physiological indices.

Imaging biomarkers of regional VH are major determinants of small airway VH markers R5-R20 and S_{acin}.

To evaluate the relationship between regional imaging measures and small airways physiology, the population was split into Low/High sub groups (Low ≤ mean, High > mean) according to absolute S_{acin} and R5-R20 values. **TABLES 2 and E3** (clinical features) and **TABLE E4** (imaging markers) summarise clinical and imaging features according to this stratification. Healthy cases predominated in the Sacin Low (9/11) and R5-R20 Low (8/11) groups, and asthmatic cases in the high groups.

Regional analysis identified that the gradient markers evaluating inferior-superior axis FRC-TLC deformation ($\overline{\Delta HU}^{IS}$ and $\overline{\Delta HU}^{IS*}$) slopes were the only markers that differed significantly in patients in the upper tertile of S_{acin} and R5-R20 when compared to the lower tertile ($p<0.05$)

[**TABLE 2**]. Specifically for both S_{acin} and R5-R20 High cases, the ventilation gradient was reversed in the inferior-superior axis ($\overline{\Delta HU}^{\mathbf{IS}}$ and $\overline{\Delta HU}^{\mathbf{IS*}}$), such that ventilation was significantly reduced at the base of the lung. This is further exemplified in **FIGURE 3**, which presents ventilation gradient maps from the base to the apex of the lung comparing cases within the upper and lower tertiles of R5-R20 and S_{acin} respectively, and two exemplar subjects with and without ventilation gradient reversal. A similar but markedly less pronounced gradient change could be seen in the posterior regions of the lower lobes (anterior-posterior axis ($\overline{\Delta HU}^{\mathbf{AP}}$)) when comparing patients with high and low clinical levels of VH (R5-R20, Sacin), demonstrating reduced posterior ventilation in the lower lobes [**FIGURE E4**].

Further examination [**FIGURE 4**] of the distribution of ΔHU and regional PRM^{fSAD}, in cases with a high and low $\overline{\Delta HU}^{\mathbf{IS*}}$, identified that patients with high $\overline{\Delta HU}^{\mathbf{IS*}}$ (ventilation gradient reversal) appeared to have focused regionalisation of lung disease (particularly *but not exclusively* in the lower lobes). In contrast patients with a low $\overline{\Delta HU}^{\mathbf{IS*}}$ had more homogeneous distributions of both ΔHU and PRM^{FSAD}.

15/16 $\overline{\Delta HU}^{\mathbf{IS*}}$ **high** cases had abnormal regional ventilation in contrast to 5/16 $\overline{\Delta HU}^{\mathbf{IS*}}$**low** cases. Regionalisation of disease in all of these cases was in the lower lobes, generally focussed at the lung bases (see arrows). A chi squared analysis of the proportions of cases with abnormal regionalisation in each group demonstrated a p-value of $p<0.0001$. ΔHU and PRM classifications correlated imperfectly [**FIGURE 4**], however lower ΔHU voxels were consistently associated with PRM^{fSAD} [**FIGURE E5**].

364 **Imaging gradient biomarkers and clinical disease**

365

366 We examined the relationship between the imaging gradient biomarkers and clinical disease
367 expression [**TABLE 2**]. We found that anterior posterior gradient imaging biomarker std
368 $(\Delta HU)^{AP}$ correlated significantly with both ACQ-6 (r = 0.33, p=0.039) and AQLQ (r=-0.34,
369 p=0.02). We also found a significant association for the inferior-superior gradient imaging
370 biomarker ($\overline{\boldsymbol{\Delta HU}}^{IS*}$) and asthma quality of life (r=-0.39, p<0.01) but not asthma control. None of
371 the gradient biomarkers were associated with exacerbation frequency.

372

373 **Discrimination of S_{acin} and R5-R20 with imaging markers of density change (ΔHU)**
374 **gradients and lung size asymmetry**

375 **FIGURE 5** and **TABLE E8** presents the results of linear discriminant analysis (LDA) which
376 sought to identify the relative contribution of spatial CT derived VH biomarkers, potential
377 clinical contributors/confounders and spirometry to physiological VH indices S_{acin} and R5-R20.
378 LDA demonstrated that the CT markers of ΔHU in the inferior-superior and anterior-posterior
379 axes as well as right to left lung size asymmetry provided the greatest overall discriminatory
380 value of small airway physiological indices, confirming that these metrics contained most of the
381 information content of the clinical small airway physiological indices.

382

383 **Computational modelling validation of CT imaging PRM gradients**

384 Computational modelling of regional bronchoconstriction in small airway patient specific
385 conducting airway models [**FIGURE 6**] identified that increasing constriction of the small
386 airways (≤ 2mm diameter), that would be most influenced by gravity in the supine posture (lower

lobe and posterior), promoted profound elevations in R5-R20 that were not seen with orthostatic simulations (i.e. constriction of small airways that would be most influenced by gravity in the orthostatic posture). Furthermore, similar regional constriction in the upper lobes did not promote the same difference on R5-R20 when considering orthostatic and supine postures. The computational models therefore provided further insight into the associations between lower lobe regional focus of disease and R5-R20 response seen in the clinical imaging study [**FIGURES 3-4]**.

394 **DISCUSSION**

395 We have performed the first quantitative functional CT imaging study to understand the spatial
396 determinant of small airway VH markers R5-R20 and S_{acin} in adult asthmatics and healthy
397 volunteers. Furthermore we have coupled CT imaging with computational simulation of small
398 airway physiology to understand the impact of disease regional pattern upon abnormal
399 physiological indices of VH.

400

401 Using a panel of imaging biomarkers **[TABLE E1]**, derived from inspiratory and expiratory CT
402 scans, we have identified that gradients in ΔHU from the base to apex of the lung are a key
403 determinant of both physiological measurements. Notably there is a reversal of the normal
404 ventilation gradient in this axis, such that ΔHU is reduced at the base of the lung in patients with
405 asthma and indeed occasionally in healthy volunteers with abnormal S_{acin} and R5-R20 values. In
406 addition we have identified that other mechanisms including anterior-posterior ΔHU gradient
407 decrease and other nonspecific regionalisation of ΔHU may underpin abnormal R5-R20 and S_{acin}
408 indices in adult asthma. We found broadly similar but not identical results with the widely
409 reported markers of small airways disease PRM^{fSAD}. Computational small airway tree models
410 were then used to confirm the impact of gravitationally dependant lower lobe disease regional
411 focus on IOS marker R5-R20, and matched our observation closely.

412

413 Previous studies have examined the difference in VH, between asthmatic and healthy subjects,
414 using hyperpolarized 3HE MRI [3], and another linked hyperpolarized 3He MRI with
415 computational models to examine airway constriction in asthma [39].We are also aware of one
416 study in bronchiectasis that attempted to correlate global burden of CT disease with

physiological indices of VH [40]. This study used correlations and regressions to identify associations between MBW lung clearance index [LCI] (a global marker of VH) and a CT scoring of the extent of bronchiectasis

Our study uses quantitative functional CT derived indices and specifically sheds insight into the topographical origins of abnormal R5-R20 (IOS derived) and S_{acin} (MBW) derived VH markers. Furthermore our observations, coupled with computer simulations [FIGURES 3-4, 6] suggest that regionalisation rather than global disease burden may be key determinants of S_{acin} and R5-R20 in asthma.

Our results are clinically important for a number of reasons. Reduced basal ventilation in asthma may be associated with reduced effective deposition of inhaled drugs, which may be a factor in poor asthma control reported in patients on ICS/LABA combination therapies in European and other populations [41]; this hypothesis would require testing with future studies. Additionally our findings are important as they are the first to use spatial and functional information derived from quantitative PRM based CT imaging to shed insight into empirical lung physiological measurements R5-R20 and S_{acin} that are widely reported as small airway dysfunction detection tools.

Interestingly we found few differences in the PRM whole lung averages for functional small airways disease, emphysema and healthy (normally deforming lung voxels) in patients with and without high levels of clinical VH derived from MBW and IOS. In contrast average whole lung PRM values were associated with airflow obstruction measured using spirometry. The latter

observations highlight both the importance of using the full information content of spatial imaging when trying to understand the topographical basis of VH indices, and the fact that expiratory flow limitation in asthma is a maker of total burden of lung unit damage rather than the heterogeneity of damage.

A likely factor of the observed ventilation gradients in the lung is the 'slinky' effect, which describes the compression of a slinky coil parallel to the gravitational field under normal gravitational conditions, isogravity and hypergravity [42]. As the dependant regions of the lung are compressed by the weight of the lung above them, they have lower end expiratory volume and the surrounding pleural pressure is more positive (in comparison to the apex), consequently a given respiratory effort and change in pleural pressure will lead to a larger increase in volume.

Other factors responsible for ventilation and perfusion gradients are likely to include lung elastic recoil, nonlinear pressure-volume relationships, the influence of large vessels, and airways closure within dependant airways. These effects have been reported in imaging studies using both protocol MRI approaches [43] and more recently a CT imaging lung deformation study in severe asthma [19].

The finding of a reverse ΔHU gradient at the base of the lung in patients with abnormal S_{acin} and R5-R20 values, and asthma, may occur as consequence of a number of factors in asthmatic patients. Specifically basal airways may close at FRC in asthma, particularly when supine, and this may reduce the specific ventilation to the lung base; one study observed results to this effect in airway constriction due to methacholine challenge [44]. Additionally the average BMI in our

cohort was 30 kg/m^2, fat distribution in the abdomen and near the base of the lung may alter diaphragmatic and basal airway mechanics and promote airways closure. Additionally it is possible that there is preferential remodelling of the airways in the lung base in asthmatics. However this would need to be confirmed by pathological studies. Similar effects including the impact of gravity may promote the smaller anterior-posterior gradient decrease seen in patients with clinical VH. It is important to note that the linear discriminant analysis identified that ventilation gradients were the best discriminant of R5-R20 independent of potential confounders such as BMI, smoking and age.

The current findings in this report add to our previous observations which have identified that both the degree and heterogeneity of small airway obstruction promote abnormal R5-R20 values [45], and that S_{acin} may be driven by asymmetries in the lung at length scales that equate to the level of the alveolar duct [9]. Specifically here we show that ventilation gradients in the lung are a major discriminant factor associated with both abnormal IOS derived R5-R20 and MBW derived S_{acin} values.

There are a number of limitations to our findings that warrant further evaluation. Firstly our study included asthmatics with a smoking pack year history of more than 15 pack years. Although these patients had no demonstrable imaging or physiological evidence of emphysema it is possible that smoking exposure rather than asthma per se was the driver of disease gradients in these patients. As a consequence larger studies are required to evaluate the gradient biomarkers reported here, across the spectrum of asthma severity and treatment intensity, and in both smoking and non-smoking asthma populations. The same limitation of sample size warrants

further evaluation of the imaging biomarkers in severe asthma populations, and considering the association of the biomarkers with patient related outcome measures in asthma. Such studies are underway and will report in due course [46]. Our imaging gradient biomarkers (derived via image registration of inspiratory and expiratory CT scans) are likely to be sensitive to both reconstruction kernel and lung volumes as reported previously [47]. However all of our CT scans were acquired at a single centre with the same reconstruction kernel and all patients were coached to expire to FRC for expiratory CT imaging prior to scanning. Nonetheless it is possible that expiratory imaging near residual volume would accentuate the imaging findings observed here and future studies are required to assess the impact of expiratory volume upon the imaging biomarkers reported here.

In conclusion, we have shown for the first time, using functional and computational approaches derived from CT imaging, that small airway VH, captured by IOS R5-R20 and MBW S_{acin}, is associated with CT density gradient reversal at the lung base, which is likely to be a direct consequence of reduced specific ventilation and small airways disease. The implications of these findings upon clinical disease expression, inhaled drug deposition and potential use in targeted inhaled drug delivery systems should now be considered in larger imaging cohorts and interventional studies.

504 **REFERENCES**

505 1) Lui JK, Lutchen KR. The role of heterogeneity in asthma: a structure-to-function perspective.
506 Clin Transl Med. 2017 Dec 1;6(1):29.

507

508 2) Teague WG, Tustison NJ, Altes TA. Ventilation heterogeneity in asthma. J Asthma. 2014 Sep
509 1;51(7):677-84.

510

511 3) Tzeng YS, Lutchen K, Albert M. The difference in ventilation heterogeneity between
512 asthmatic and healthy subjects quantified using hyperpolarized 3He MRI. J Appl Physiol. 2009
513 Mar;106(3):813-22.

514

515 4) Tahir BA, Van Holsbeke C, Ireland RH, Swift AJ, Horn FC, Marshall H, et al. Comparison of
516 CT-based lobar ventilation with 3He MR imaging ventilation measurements. Radiology. 2015
517 Aug 28;278(2):585-92.

518

519 5) Zha W, Kruger SJ, Johnson KM, Cadman RV, Bell LC, Liu F, et al. Pulmonary ventilation
520 imaging in asthma and cystic fibrosis using oxygen□enhanced 3D radial ultrashort echo time
521 MRI. J Magn Reson Imaging. 2018 May;47(5):1287-97.

522

6) Venegas J, Winkler T, Harris RS. Lung physiology and aerosol deposition imaged with positron emission tomography. J Aerosol Med Pulm Drug Deliv. 2013 Feb 1;26(1):1-8.

7) Farrow CE, Salome CM, Harris BE, Bailey DL, Berend N, King GG. Peripheral ventilation heterogeneity determines the extent of bronchoconstriction in asthma. J Appl Physiol. 2017 Aug 10;123(5):1188-94.

8) Verbanck S, Paiva M. Gas mixing in the airways and airspaces. Compr Physiol. 2011 Apr;1(2):809-34.

9) Gonem S, Hardy S, Buhl N, Hartley R, Soares M, Kay R, et al. Characterization of acinar airspace involvement in asthmatic patients by using inert gas washout and hyperpolarized 3helium magnetic resonance. J Allergy Clin Immunol. 2016 Feb 1;137(2):417-25.

10) Galant SP, Komarow HD, Shin HW, Siddiqui S, Lipworth BJ. The case for impulse oscillometry in the management of asthma in children and adults. Ann Allergy Asthma Immunol. 2017 Jun 1;118(6):664-71.

11) Gonem S, Natarajan S, Desai D, Corkill S, Singapuri A, Bradding P, et al. Clinical significance of small airway obstruction markers in patients with asthma. Clin Exp Allergy. 2014 Apr 1;44(4):499-507.

12) Oostveen E, MacLeod D, Lorino H, Farre R, Hantos Z, Desager K, et al. The forced oscillation technique in clinical practice: methodology, recommendations and future developments. Eur Respir J. 2003 Dec 1;22(6):1026-41.

13) Robinson P, Latzin P, Verbanck S, Hall GL, Horsley A, Gappa M, et al. Consensus statement for inert gas washout measurement using multiple and single breath tests. Eur Respir J. 2012 Jan 1:erj00697-2012.

14) Farah CS, King GG, Brown NJ, Downie SR, Kermode JA, Hardaker KM, et al. The role of the small airways in the clinical expression of asthma in adults. J Allergy Clin Immunol. 2012 Feb 1;129(2):381-7.

15) Thompson BR, Douglass JA, Ellis MJ, Kelly VJ, O'hehir RE, King GG, et al. Peripheral lung function in patients with stable and unstable asthma. J Allergy Clin Immunol. 2013 May 1;131(5):1322-8.

16) Galvin I, Drummond GB, Nirmalan M. Distribution of blood flow and ventilation in the lung: gravity is not the only factor. Br J Anaesth. 2007 Apr 1;98(4):420-8.

17) Gupta S, Hartley R, Khan UT, Singapuri A, Hargadon B, Monteiro W, et al. Quantitative computed tomography–derived clusters: redefining airway remodeling in asthmatic patients. J Allergy Clin Immunol. 2014 Mar 1;133(3):729-38.

568 18) Shim SS, Schiebler ML, Evans MD, Jarjour N, Sorkness RL, Denlinger LC, et al. Lumen
569 area change (Delta Lumen) between inspiratory and expiratory multidetector computed
570 tomography as a measure of severe outcomes in asthmatic patients. J Allergy Clin Immunol.
571 2018 Feb 10. pii: S0091-6749(18)30219-7.
572
573 19) Choi S, Hoffman EA, Wenzel SE, Tawhai MH, Yin Y, Castro M, et al. Registration-based
574 assessment of regional lung function via volumetric CT images of normal subjects vs. severe
575 asthmatics. J Appl Physiol. 2013 Jun 6;115(5):730-42.
576
577 20) Galbán CJ, Han MK, Boes JL, Chughtai KA, Meyer CR, Johnson TD, et al. Computed
578 tomography–based biomarker provides unique signature for diagnosis of COPD phenotypes and
579 disease progression. Nat Med. 2012 Nov;18(11):1711.
580
581 21) Boes JL, Hoff BA, Bule M, Johnson TD, Rehemtulla A, Chamberlain R, et al. Parametric
582 response mapping monitors temporal changes on lung CT scans in the subpopulations and
583 intermediate outcome measures in COPD Study (SPIROMICS). Acad Radiol. 2015 Feb
584 1;22(2):186-94.
585
586 22) Bhatt SP, Soler X, Wang X, Murray S, Anzueto AR, Beaty TH, et al. Association between
587 functional small airway disease and FEV1 decline in chronic obstructive pulmonary disease. Am
588 J Respir Crit Care Med. 2016 Jul 15;194(2):178-84.
589
590 23) 2018 GINA Report, Global Strategy for Asthma Management and Prevention. Available at:

https://ginasthma.org/2018-gina-report-global-strategy-for-asthma-management-and-prevention/. Accessed January 9, 2019.

24) Heaney LG, Brightling CE, Menzies-Gow A, Stevenson M, Niven RM. Refractory asthma in the UK: cross-sectional findings from a UK multicentre registry. Thorax. 2010 Sep 1;65(9):787-94.

25) Juniper EF, Svensson K, Mörk AC, Ståhl E. Measurement properties and interpretation of three shortened versions of the asthma control questionnaire. Respir Med. 2005 May 1;99(5):553-8.

26) Juniper EF, Buist AS, Cox FM, Ferrie PJ, King DR. Validation of a standardized version of the Asthma Quality of Life Questionnaire. Chest. 1999 May 1;115(5):1265-70.

27) Reddel HK, Taylor DR, Bateman ED, Boulet LP, Boushey HA, Busse WW, et al.. An official American Thoracic Society/European Respiratory Society statement: asthma control and exacerbations: standardizing endpoints for clinical asthma trials and clinical practice. Am J Respir Crit Care Med. 2009 Jul 1;180(1):59-99.

28) Miller MR, Hankinson JA, Brusasco V, Burgos F, Casaburi R, Coates A, et al. Standardisation of spirometry. Eur Respir J. 2005 Aug 1;26(2):319-38.

29) Dutrieue B, Vanholsbeeck F, Verbanck S, Paiva M. A human acinar structure for simulation

614 of realistic alveolar plateau slopes. J Appl Physiol. 2000 Nov 1;89(5):1859-67.

615

616 30) Wanger J, Clausen JL, Coates A, Pedersen OF, Brusasco V, Burgos F, et al. Standardisation
617 of the measurement of lung volumes. Eur Respir J. 2005 Sep 1;26(3):511-22.

618

619 31) MacIntyre N, Crapo R, Viegi G, Johnson DC, Van Der Grinten CP, Brusasco V, et al.
620 Standardisation of the single-breath determination of carbon monoxide uptake in the lung. Eur
621 Respir J. 2005; 26: 720–735.

622

623 32) Benade AH. On the propagation of sound waves in a cylindrical conduit. J Acoust Soc Am.
624 1968 Aug;44(2):616-23.

625

626 33) Kaczka DW, Massa CB, Simon BA. Reliability of estimating stochastic lung tissue
627 heterogeneity from pulmonary impedance spectra: a forward-inverse modeling study. Ann
628 Biomed Eng. 2007 Oct 1;35(10):1722-38.

629

630 34) Lutchen KR, Gillis H. Relationship between heterogeneous changes in airway morphometry
631 and lung resistance and elastance. J Appl Physiol. 1997 Oct 1;83(4):1192-201.

632

633 35) Bhatawadekar SA, Leary D, Maksym GN. Modelling resistance and reactance with
634 heterogeneous airway narrowing in mild to severe asthma. Can J Physiol Pharmacol. 2015 Jan
635 21;93(3):207-14.

636

637 36) Cauberghs M, Van de Woestijne KP. Mechanical properties of the upper airway. J Appl
638 Physiol. 1983 Aug 1;55(2):335-42.

639

640 37) Bordas R, Lefevre C, Veeckmans B, Pitt-Francis J, Fetita C, Brightling CE, et al.
641 Development and Analysis of Patient-Based Complete Conducting Airways Models. PLOS
642 ONE. 2015 Dec 11;10(12):e0144105.

643

644 38) Boudewijn IM, Postma DS, Telenga ED, ten Hacken NH, Timens W, Oudkerk M, et al.
645 Effects of ageing and smoking on pulmonary computed tomography scans using parametric
646 response mapping. Eur Respir J. 2015 Jun 25:ERJ-00094.

647

648 39) Campana L, Kenyon J, Zhalehdoust-Sani S, Tzeng YS, Sun Y, Albert M, et al. Probing
649 airway conditions governing ventilation defects in asthma via hyperpolarized MRI image
650 functional modeling. J Appl Physiol. 2009 Apr;106(4):1293-300.

40) Verbanck S, King GG, Zhou W, Miller A, Thamrin C, Schuermans D, et al. The quantitative link of lung clearance index to bronchial segments affected by bronchiectasis. Thorax. 2017 Sep 2:thoraxjnl-2017.

41) Partridge MR, van der Molen T, Myrseth SE, Busse WW. Attitudes and actions of asthma patients on regular maintenance therapy: the INSPIRE study. BMC Pulm Med. 2006 Dec;6(1):13.

42) Hopkins SR, Henderson AC, Levin DL, Yamada K, Arai T, Buxton RB, et al. Vertical gradients in regional lung density and perfusion in the supine human lung: the Slinky effect. J Appl Physiol. 2007 Jul;103(1):240-8.

43) Henderson AC, Sá RC, Theilmann RJ, Buxton RB, Prisk GK, Hopkins SR. The gravitational distribution of ventilation-perfusion ratio is more uniform in prone than supine posture in the normal human lung. J Appl Physiol. 2013 Apr 25;115(3):313-24.

44) Soares M, Bordas R, Thorpe J, Timmerman B, Brightling C, Kay D, et al. Validation of impulse oscillometry R5-R20 as a small airways dysfunction detection tool in adult asthma. Eur Respir J. 2016 48: OA4968.

672 45) Farrow CE, Salome CM, Harris BE, Bailey DL, Bailey E, Berend N, et al. Airway closure on
673 imaging relates to airway hyper responsiveness and peripheral airway disease in asthma. J Appl
674 Physiol. 2012 Jul 26;113(6):958-66.

675

676 46) Postma DS, Brightling C, Fabbri L, van der Molen T, Nicolini G, Papi A, et al. Unmet needs
677 for the assessment of small airways dysfunction in asthma: introduction to the ATLANTIS study.
678 Eur Respir J. 2015 Jun;45(6):1534-8.

679

680 47) Boes JL, Bule M, Hoff BA, Chamberlain R, Lynch DA, Stojanovska J, et al. The Impact of
681 Sources of Variability on Parametric Response Mapping of Lung CT Scans. Tomography. 2015
682 Sep;1(1):69-77.

683 **TABLES**

684 **Table 1.** Clinical characteristics of asthmatic and healthy subjects.

		Asthma			
	Healthy volunteers (n=11)	**All** (n=41)	**GINA 1** (n=8)	**GINA 2/3** (n=20)	**GINA 4/5** (n=13)
Clinical					
Age (years)	54.1 (± 14.4)	53.7 (± 12.6)	53.0 (± 9.2)	56.5 (± 12.8)	49.7 (± 13.7)
Sex [male/female]	[6/5]	[18/23]	[3/5]	[10/10]	[5/8]
BMI ($Kg.m^2$)	28.8 (± 4.5)	27.1 (± 4.9)	25.2 (± 4.4)0	26.3 (± 4.6)	29.4 (± 5.3)
Atopic [Yes/No]	$[3/8]_{1,2}$	[30/11]	$[6/2]_{H}$	$[16/4]_{H}$	[8/5]
Smoking (pack years)	4.2 (± 7.8)	7.3 (± 17.0)	3.0 (± 4.9)	5.0 (± 8.1)	13.4 (± 27.9)
No. of exacerbations. (past 12 months)	-	1.4 (± 2.1)	0.5 (± 0.8)	1.1 (± 2.3)	2.2 (± 2.1)
ACQ-6	-	1.27 (± 1.04)	0.94 (± 0.85)	1.22 (± 0.85)	1.56 (± 1.35)
AQLQ	-	5.37 (± 1.11)	5.94 (± 0.90)	5.28 (± 1.21)	5.15 (± 1.00)
Asthma Duration (years)	-	17.6 (± 16.7)	13.3 (± 9.5)	18.9 (± 18.3)	18.2 (± 18.2)
Beclamethasone Diproprionate Equivalent. ICS Dose (micrograms/24 hours)	-	820 (± 698)	100. (± $282)_{2,3}$	650 (± $371)_{1,3}$	1523 (± $656)_{1,2}$
Physiology					
Post-BD FEV_1(L)	3.7 (± $1.0)_{A,1,2}$	2.7 (± $0.80)_{H}$	2.5 (± $0.68)_{H}$	2.8 (± $0.85)_{H}$	2.7 (± 0.81)
Post-BD FEV_1%	116 (± $19)_{A}$	97.2 (± $20)_{H}$	99.5 (± 20.8)	97.7 (± 15.5)	95.1 (± 26.3)
Post-BD FEV_1/FVC (%)	80 (± 3.2)	74 (± 11)	76 (± 11)	76 (± 7.6)	72 (± 15)
Bronchodilator Response (% FEV_1)	3.62 (± $3.38)_{A}$	12.88 (± $16.33)_{H}$	8.79 (± 8.19)	11.31 (± 13.52)	17.80 (± 22.77)
RV/TLC (%)	32.10 (±$7.71)_{A}$	38.83 (± $8.68)_{H}$	38.36 (± 8.41)	40.43 (± 9.65)	36.48 (± 7.13)

KCO % pred	96.15 (± 12.69)$_{A}$	104.65 (± 15.78)$_{H}$	101.13 (± 14.68)	108.30 (± 15.53)	100.92 (± 16.77)
Multiple Breath Washout					
LCI	7.32 (± 1.01)	7.80 (± 1.28)	7.51 (± 1.93)	7.75 (± 1.01)	8.05 (± 1.24)
S_{acin}	0.131 (± 0.052)$_{A}$	0.207 (± 0.116)$_{H}$	0.193 (± 0.185)	0.203 (± 0.097)	0.220 (± 0.097)
S_{cond}	0.037 (± 0.034)	0.035 (± 0.024)	0.034 (± 0.026)	0.039 (± 0.026)	0.028 (± 0.018)
Impulse Oscillometry					
R5-R20 (Kpa.s.L^{-1})	0.033 (± 0.029)	0.061 (± 0.058)	0.055 (± 0.035)	0.053 (± 0.042)	0.077 (± 0.085)
AX (Kpa/L)	0.291 (± 0.219)$_{A}$	0.639 (± 0.752)$_{H}$	0.555 (± 0.423)	0.457 (± 0.298)	0.971 (± 1.209)
Induced Sputum					
Eosinophils (%)	0.46 (± 0.30)$_{A,2}$	10.14 (± 28.17)$_{H}$	#	12.94 (± 35.70)$_{H}$	6.17 (± 6.76)
Neutrophils (%)	46.32 (± 15.68)	59.73 (± 24.47)	37.13 (± 15.55)	61.72 (± 27.02)	63.96 (± 19.12)

LEGEND: M, male; F, female; BMI, body mass index; FEV, forced expiratory volume; FVC, forced vital capacity; BD, bronchodilator; LCI, lung clearance index; AX, area of reactance. Data expressed as mean (± standard deviation). Attribute normality was tested using one-sample Kolmogorov-Smirnov test over all subjects. Binary group comparisons ('healthy' vs 'all asthmatics') were performed using two sample t-tests for parametric variables, and Mann-Whitney U-tests for non-parametric variables. Non-intersecting group comparisons were performed using one-way ANOVA for parametric variables, and Kruskal-Wallis test for non-parametric variables. Multiple-comparison procedures were performed with Turkey's honest significant difference criterion. Groups with significant separation ($p < 0.05$) indicated by subscripts A (all asthma), H (healthy control), 1, 2, 3 (GINA 1, 2/3 and 4/5 respectively) and * (all other groups).

696 **Table 2.** Computed tomography imaging biomarkers and ventilation heterogeneity based
697 stratification.

	S_{acin}		R5-R20	
	Low (n=29)	**High** (n=23)	**Low** (n=32)	**High** (n=20)
Clinical				
Asthma/Healthy	[20/9]	[21/2]	[24/8]	[17/3]
Parametric Response Mapping				
$\%PRM^{Norm}$	0.74 (± 0.11)	0.71 (± 0.14)	0.72 (± 0.14)	0.73 (± 0.09)
$\%PRM^{fSAD}$	0.19 (± 0.10)	0.19 (± 0.12)	0.19 (± 0.12)	0.18 (± 0.08)
$\%PRM^{Emph}$	0.024 (± 0.018)	0.038 (± 0.037)	0.032 (± 0.033)	0.028 (± 0.021)
$\%PRM^{Uncl}$	0.046 (± 0.036)	0.063 (± 0.030)	0.053 (± 0.038)	0.055 (± 0.028)
Parametric Response Map Ellipse Properties				
ellMajL	126.2 (± 30.0)	130.2 (± 28.9)	122.0 (± 28.3)	137.5 (± 29.0)
ellMinL †	55.1 (± 9.4)	56.5 (± 11.8)	**52.1 (± 9.1)**	**61.4 (± 10.0)**
ellArea †	5590 (± 2067)	5922 (± 2251)	**5092 (± 1763)**	**6769 (± 2312)**
ellAngle	0.21 (± 0.13)	0.16 (± 0.09)	0.19 (± 0.11)	0.20 (± 0.11)
Ventilation gradient (ΔHU)				
$std(\Delta HU)^{AP}$	0.070 (± 0.078)	0.059 (± 0.057)	0.055 (± 0.068)	0.080 (± 0.070)
$\overline{\Delta HU}^{AP}$ †	0.473 (± 0.207)	0.450 (± 0.234)	**0.512 (± 0.226)**	**0.386 (± 0.183)**
$std(\Delta HU)^{IS}$ *	**-0.077 (± 0.043)**	**-0.046 (±0.035)**	-0.064 (± 0.040)	-0.062 (± 0.047)
$\overline{\Delta HU}^{IS}$ *,†	**-0.043 (± 0.112)**	**0.021 (± 0.099)**	**-0.051 (± 0.100)**	**0.044 (± 0.102)**
$\overline{\Delta HU}^{IS*}$ *,†	**-2.033 (± 4.372)**	**0.489 (± 3.936)**	**-2.282 (± 4.018)**	**1.267 (± 3.987)**

698

699 LEGEND: PRM, Parametric Response Map; SAA, Stratified Axial Analysis; Data expressed as mean

(standard deviation). Attribute normality was tested using one-sample Kolmogorov-Smirnov test over all subjects. Binary group (i.e. S_{acin} low vs. S_{acin} high, and R5-R20 low vs. R5-R20 high) comparisons were performed using two sample t-tests for parametric variables, and Mann-Whitney U-tests for non-parametric variables. Groups with significant separation ($p < 0.05$) of S_{acin} (R5-R20) indicated by * (†).

704 **FIGURE LEGENDS**

705 **FIGURE 1.** Global parametric response (PRM) mapping and spirometry. A: PRM features based
706 on TLC and FRC HU joint density histogram (JDH). PRM voxel classification (left) defined by
707 lines of expiration HU = -856 and inspiration HU = -950 utilised for defining PRM^{fSAD} and PRM
708 ellipse geometry. B, JDH visualisation of FEV_1/FVC (%) extreme cases, demonstrating compact
709 and left shifted ellipses in patients with airflow obstruction. C, box plot illustrating that patients
710 with spirometric airflow obstruction have smaller PRM ellipse areas and significantly more
711 functional small airways disease on CT imaging $\%PRM^{fSAD}$; groups formed about median
712 $FEV_1/FVC(\%)$.

713

714 **FIGURE 2.** Overview of the slinky effect in the lungs in the standing and supine postures
715 demonstrating the distribution of lung density as a consequence of gravity (A, B). It can
716 therefore be seen that in the supine posture the inferior-superior lung density profile will be
717 largely independent of gravity (C: transverse cross section of expiratory HU voxels) with
718 expected largest volume of ventilation in the lower lobes due to the lower lobe having the largest
719 proportionate lung volume, in contrast the anterior-posterior lung density profile will be
720 predominantly influenced by gravity (D: coronal cross section of expiratory HU voxels) such
721 that posterior ventilation will be proportionately lower than anterior ventilation.
722 The gradients of ΔHU in these two axes were used to understand the determinants of clinical
723 ventilation heterogeneity measurements derived from IOS and MBW.

724

725 **FIGURE 3.** Inferior-superior ΔHU gradient analysis in patients with a high/low S_{acin} and R5-
726 R20. A, decile-wise comparison of ΔHU mean differences, in the inferior-to-superior direction,

of groups formed from the lower and upper tertiles of S_{acin} and R5-R20 distributions, specifically the lowest and highest 16 subjects with respect to these two markers. The inferior regions show significant differences when comparing lower and upper tertiles for both S_{acin} and R5-R20. B, joint density histogram of voxel mean ΔHU and PRM^{fSAD} percentage when projected onto coronal plane in subject showing typical (healthy) ventilation (surrogated by ΔHU) pattern and homogenous PRM^{fSAD}. C, as in B in a subject with abnormal ventilation pattern and basally focused PRM^{fSAD}. Colour bars labelled with min and max of occurring mean values. D, the concept of the inferior-superior gradient reversal phenotype is summarised in a simple visual schematic.

FIGURE 4. Coronal section heat maps of ΔHU and PRM^{fSAD} in $\overline{\Delta HU}^{IS*}$ low (no gradient reversal) and high (basal gradient reversal) tertiles of total population (n=52). The images labelled with an ID number assigned with respect to decreasing $\overline{\Delta HU}^{IS*}$ values. e.g. 1 = greatest $\overline{\Delta HU}^{IS*}$ (highest level of inferior/lower zone gradient reversal), 32 = smallest $\overline{\Delta HU}^{IS*}$ (lowest level of basal gradient reversal). H indicates non-asthmatic, G indicates asthmatic, with GINA level. It can be seen that patients with high $\overline{\Delta HU}^{IS*}$ values more often than not have inferior gradient reversal but also exhibit ΔHU and PRM^{fSAD} heterogeneity. In contrast patients with a low $\overline{\Delta HU}^{IS*}$ appear to have more homogeneous distributions of ΔHU and PRM^{fSAD} or upper lobe regionalisation of low ΔHU, as would be expected in the supine posture. Colour bar ranges determined per subject based on feature (ΔHU or PRM^{fSAD}) mean and variance as indicated. Arrows highlight specific disease regionalisation in $\overline{\Delta HU}^{IS*}$ abnormal subjects. Asterisks indicate subjects selected for chi squared test of proportions, having abnormal regionalisation of ventilation.

FIGURE 5. Histograms of linear discriminant analysis (LDA) applied to the total population (n=52), illustrating best linear separation of clinical ventilation heterogeneity (VH), R5-R20 and S_{acin}. Limited additional discrimination is added when considering potential clinical confounders of VH (e.g. age, height and weight) and spirometry appears to be less sensitive at discriminating patients with normal and abnormal clinical VH than CT imaging.

FIGURE 6: Comparison of R5-R20 under varying regional small airway constrictions applied to healthy lung structure. The response of R5-R20 can be seen for homogeneous (A, C) and heterogeneous (B, D) constriction of the small airways. In each case constrictions were applied to the lowest or highest 25% of airways, relative to the orthostatic or supine position. It can be seen that lower zone constriction and regionalisation produces far greater elevations in R5-R20 than upper lobe constriction and regionalisation, in keeping with the observations in FIGURES 3 and 4.

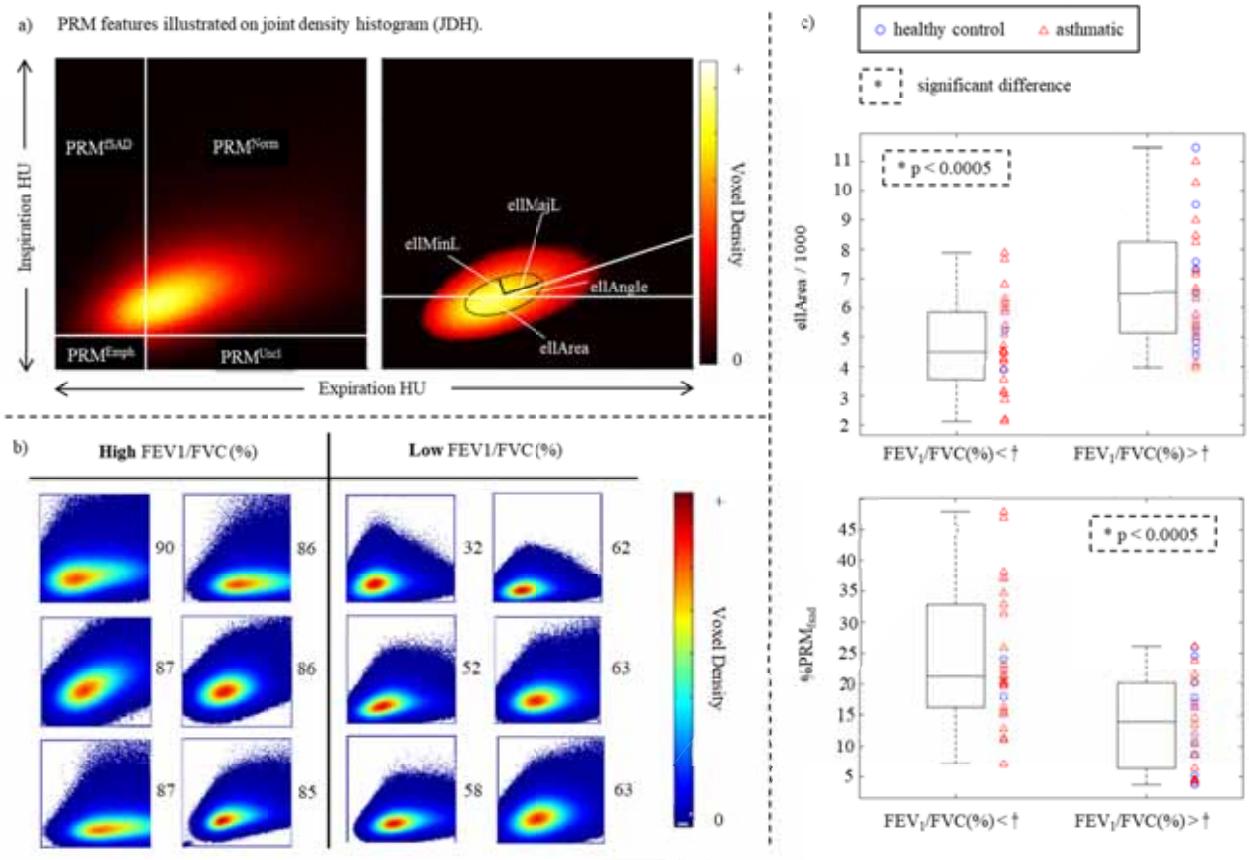

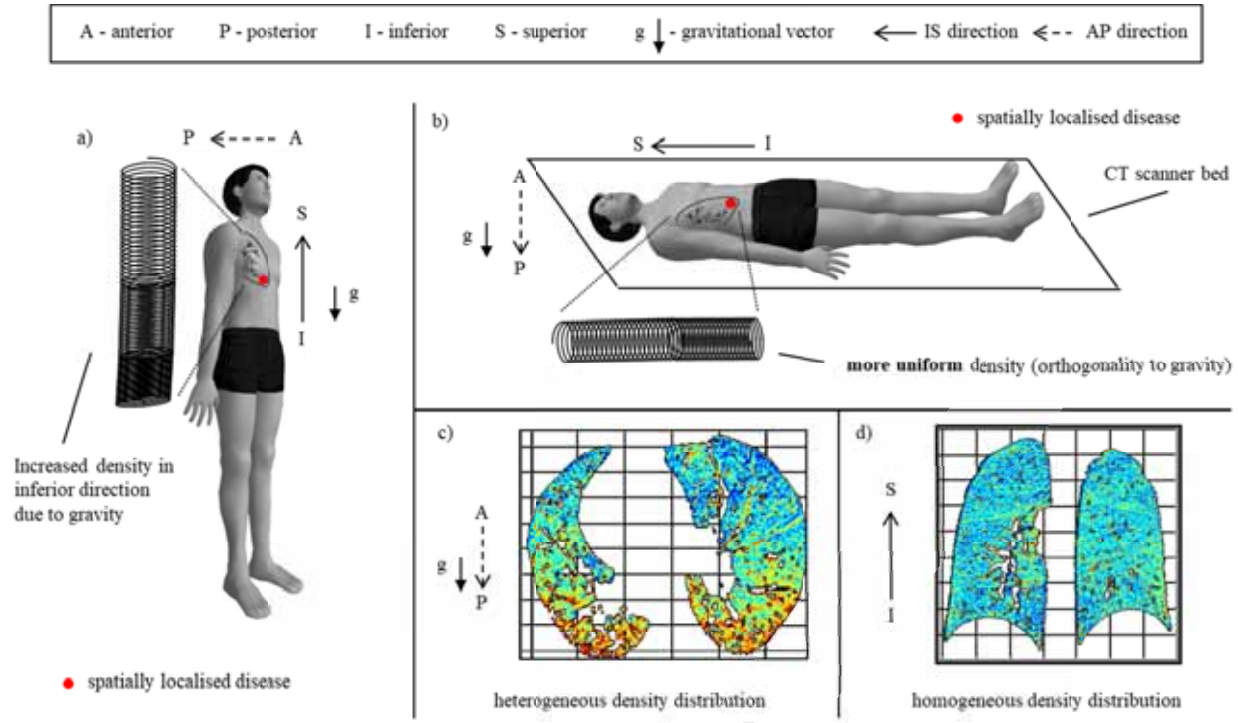

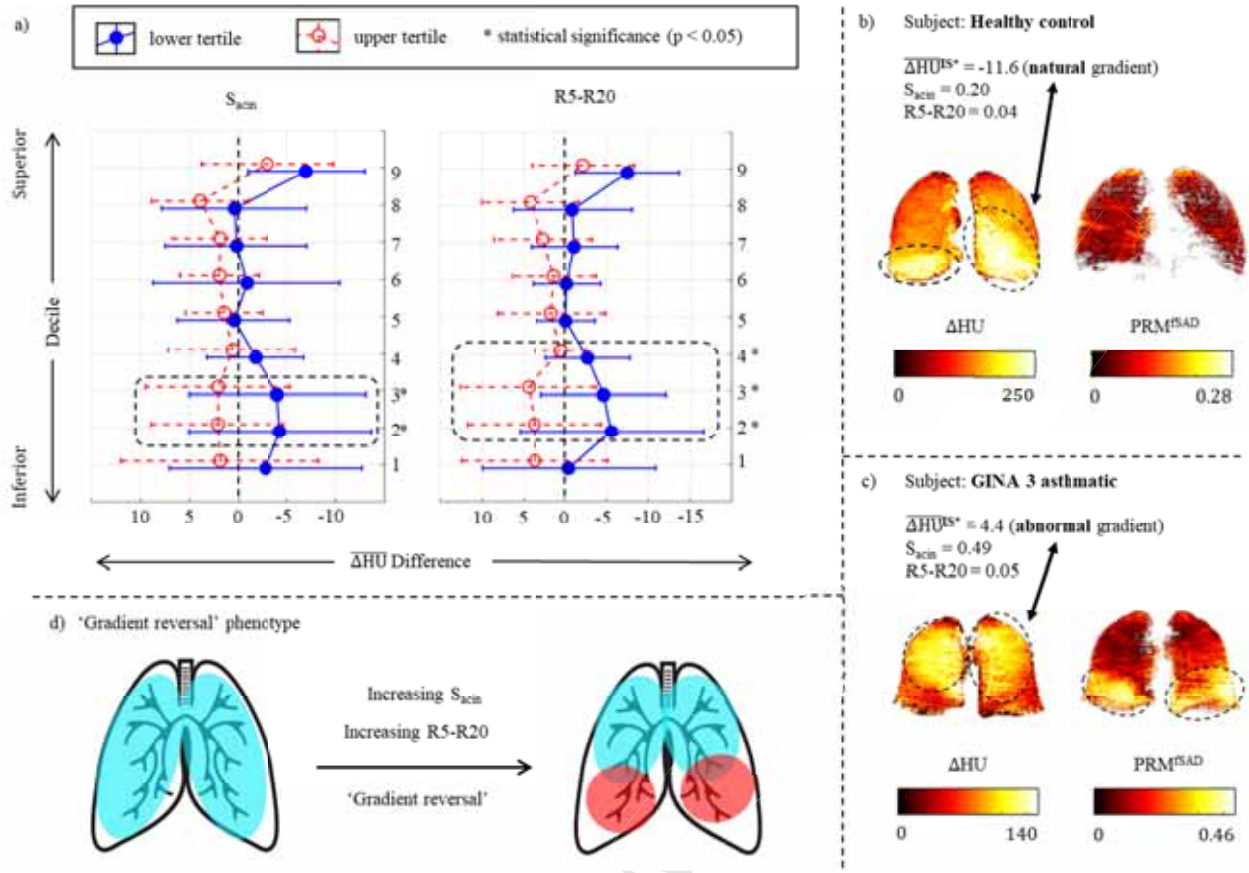

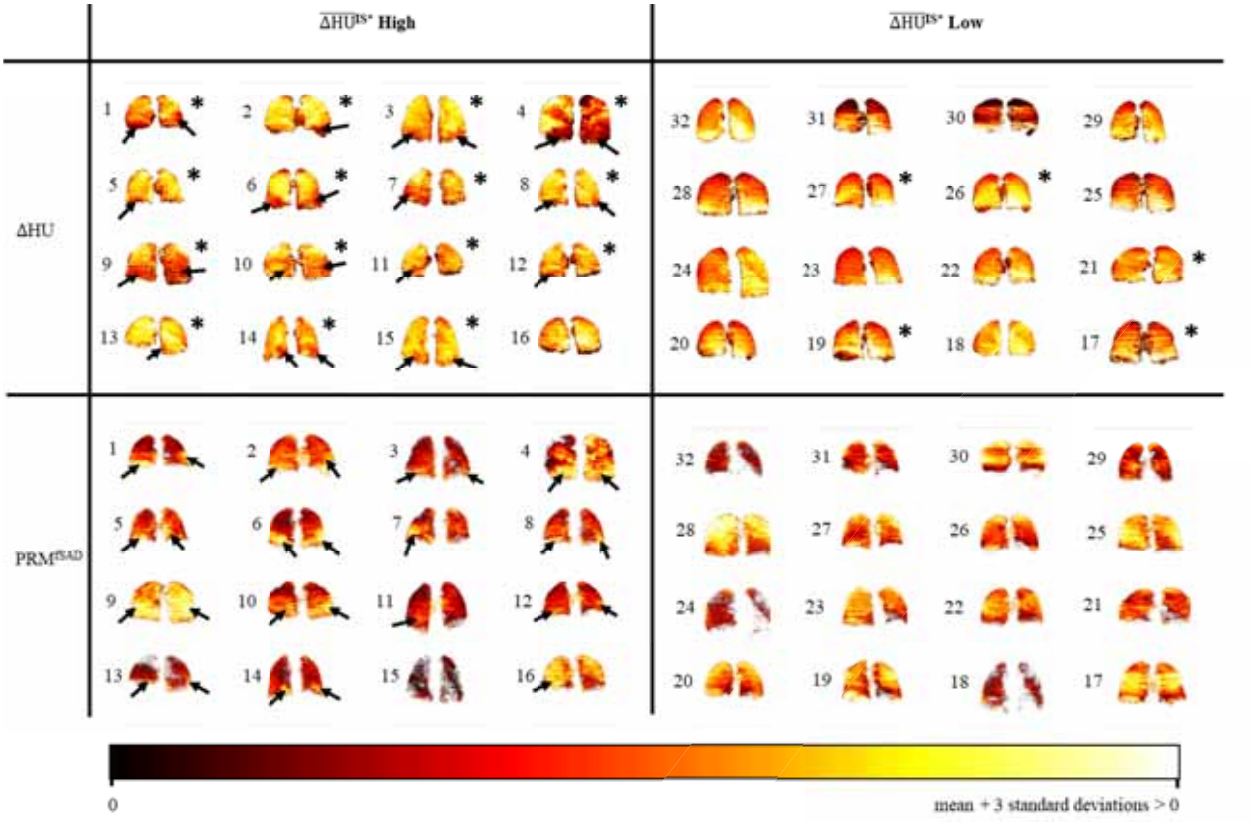

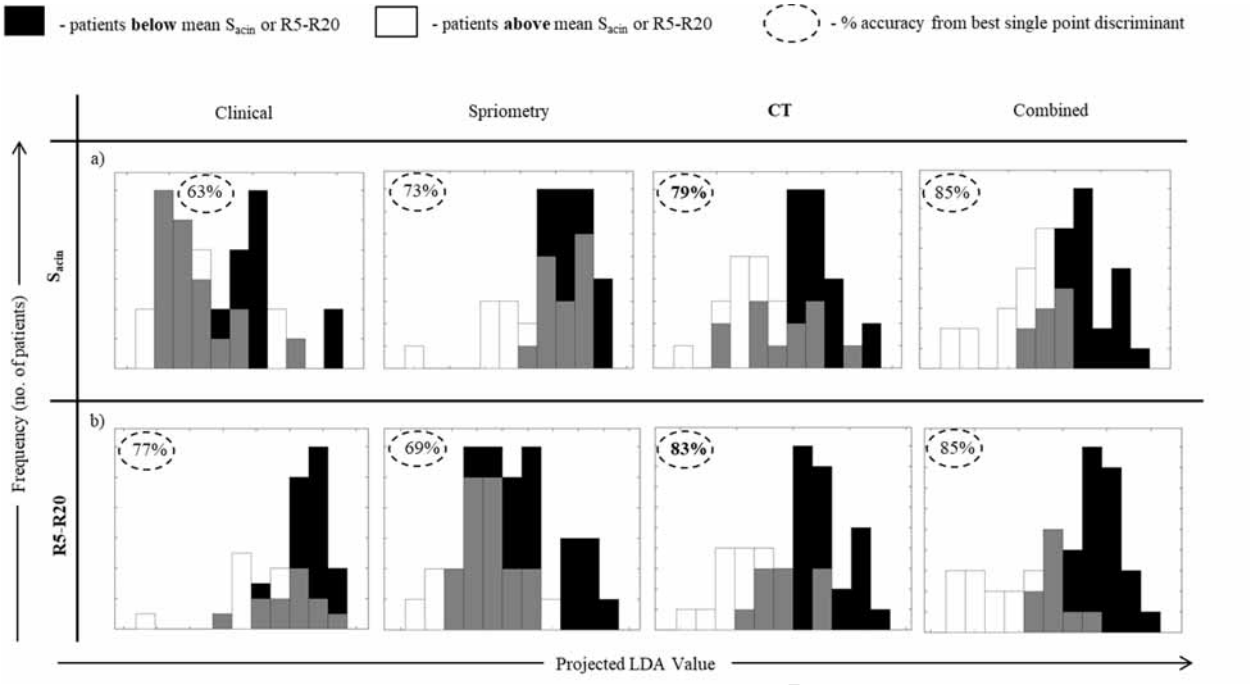

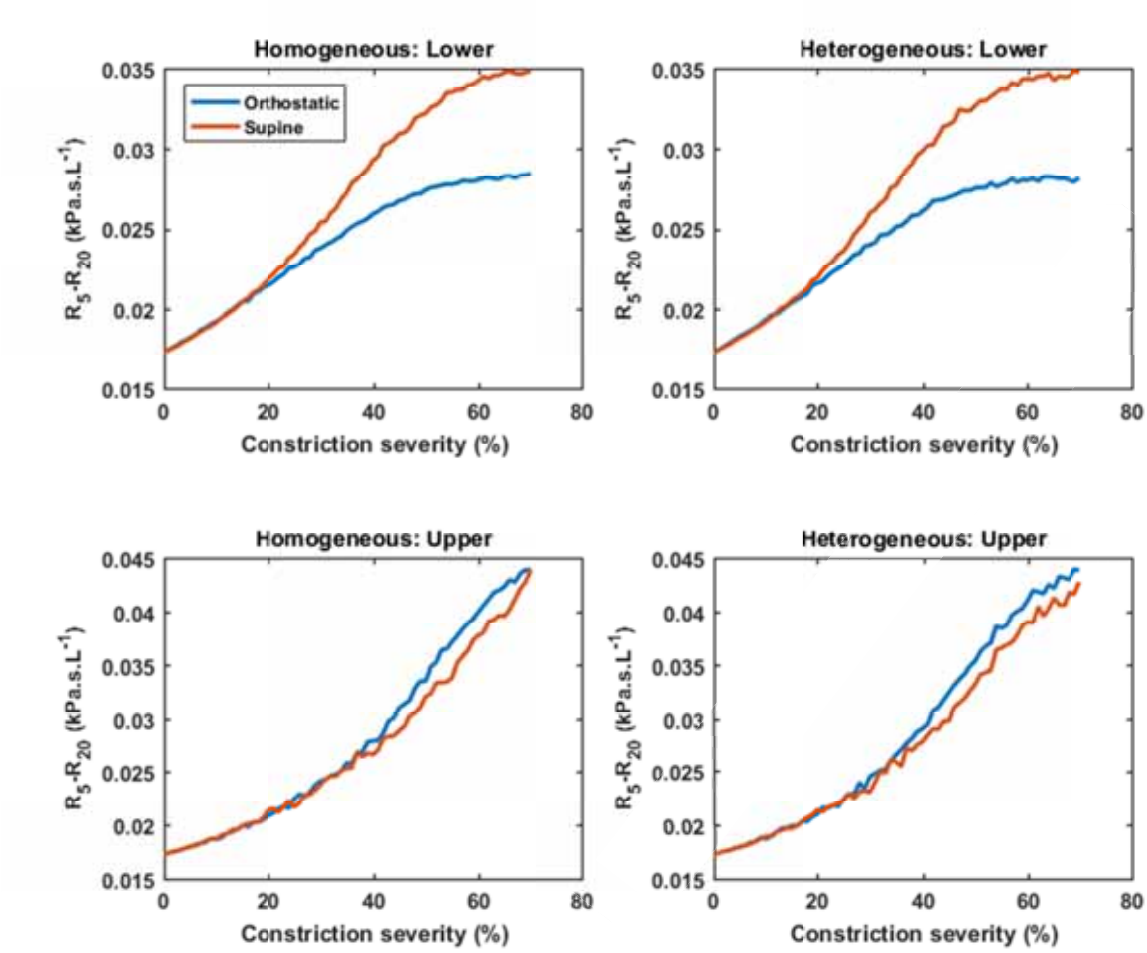
Homogeneous: Lower
Orthostatic
Supine
R_5-R_{20} (kPa.s.L^{-1})
Constriction severity (%)
Heterogeneous: Lower
Homogeneous: Upper
Heterogeneous: Upper

ONLINE REPOSITORY

Functional CT Imaging for Identification of the Spatial Determinants of Small Airways Disease in Adult Asthma

Alex J. Bell, MMath,[a] Brody H. Foy, BMath,[b] Dr. Matthew Richardson, PhD,[a] Amisha Singapuri, BSc,[a] Dr. Evgeny Mirkes PhD,[c] Dr. Maarten van den Berge, PhD, [d] Prof. David Kay, PhD, [b] Prof. Chris Brightling, FRCP, PhD, [a] Prof. Alexander N. Gorban, PhD,[c] Prof. Craig J. Galbán, PhD,[e] Prof. Salman Siddiqui, MRCP, PhD.[a]

[a]NIHR Respiratory Biomedical Research Centre (BRC), Department of Infection, Immunity and Inflammation, University of Leicester, Leicester, UK. [b]Computational Biology, Department of Computer Science, University of Oxford, Oxford, United Kingdom. [c]Department of Mathematics, University of Leicester, Leicester, UK. [d]Department of Pulmonology, University Medical Centre Groningen, Groningen, Netherlands. [e]Department of Radiology, University of Michigan, Michigan, USA.

Corresponding author

Professor Salman Siddiqui, MRCP, PhD

NIHR Biomedical Research Centre (Respiratory Theme)

Respiratory BRU Building

Glenfield Hospital

Groby Road, Leicester, LE3 9QP, UK

24 Telephone: +44-116-250-2873

25 Fax: 0116-250-2787

26 E-mail: ss338@leicester.ac.uk

27

METHODS

M1.0 Lung Function Measurements

All physiological tests were performed in the seated position by individuals with appropriate training and accreditation. Physiological tests were performed 15 mins after administration of a short-acting bronchodilator (salbutamol 400 μg). This was administered via a metered dose inhaler and spacer, with each 100 microgram actuation being inhaled in a separate inhalation to TLC, followed by a 5- to 10-s breath-hold.

Impulse oscillometry (IOS) was performed in triplicate according to standard guidelines[E1]. A volume calibration was performed daily using a 3-L syringe, and the accuracy of resistance measurements was confirmed daily using a standard 0.2 $kPaL^{-1}s$ resistance mesh. Participants wore a nose clip and supported their cheeks, while an impulse waveform was delivered to their respiratory system via a loudspeaker connected to a mouthpiece, during 60 seconds of tidal breathing. Resistance at 5 Hz (R5), resistance at 20 Hz (R20), R5-R20, reactance at 5 Hz (X5) and AX were derived from pressure and flow measurements recorded throughout the 60-second period.

Multiple breath inert gas washout (MBW) was performed in triplicate according to current guidelines[E2], using the method described by Horsley et al.[E3]. Volume calibration of the pneumotachograph was performed daily using a 1-L syringe. Participants wore a nose clip and breathed an air mixture containing 0.2% SF_6, while respiratory flows and exhaled breath SF_6 concentrations were monitored by an Innocor photoacoustic gas analyser (Innovision A/S, Odense, Denmark). Participants maintained a steady respiratory rate of approximately 12 breaths

per minute, and a constant tidal volume of 1L, using a real-time visual display of inspired volume as a guide. Once inhaled and exhaled SF_6 concentrations had equalized, participants were switched to breathing room air during an expiration and asked to continue breathing at the same respiratory rate and tidal volume. The test was terminated once the end-tidal concentration of SF_6 in exhaled breath reached less than 1/40th of the original concentration (0.005%) for three consecutive breaths. The parameters S_{cond} and S_{acin}^{E4} were calculated using custom software written with TestPoint (Measurement Computing Corporation, Norton, MA, USA).

M2.0 CT Imaging and Image Analysis

Volumetric whole-lung scans were obtained with a Siemens Sensation 16 scanner with the following low-dose protocol: 16 × 0.75mm collimation, 1.5-mm pitch, 120 kVp, 40 mA, 0.5-second rotation time, and scanning field of view of 500 mm, with dose modulation off. Scans were obtained at full inspiration and at functional residual capacity. Images were reconstructed with a slice thickness of 0.75mm at a 0.5mm interval by using B35f kernel.

Registration of the inspiratory (at total lung capacity, TLC) and expiratory (at functional residual capacity, FRC) dicom (Digital Imaging and Communications in Medicine) series was performed at the University of Michigan (USA), using Imbio's Lung Density Analysis (LDA™) software application (Imbio, LLC, Minneapolis, MN). The software automatically segments lung volumes (excluding the major airways, up to approximately 3-4 generations from the trachea), taking series with least volume as expiration set, and calculates a warping function T to approximate regional deformation between expiration and inspiration states. Registration is then performed inspiration-to-expiration (I2E), that is, a voxel v in the expiration image is linked to a set of

voxels in the inspiration image based on T(v). This provides an assignment of both expiratory Hounsfield unit (HU), i.e. HU of v, and inspiratory HU, i.e. mean HU of set captured by T(v), to a single point in space, specified by Cartesian coordinates (x,y,z). N.B. axes of coordinate system are determined by the CT scanner.

CT data was provided to the University of Leicester (UK) in the form of $n \times 5$ matrices, where n is the number of voxels, and the 5 columns cover Cartesian coordinates (3 attributes, x, y and z) and HU value at expiration and inspiration (2 attributes, expiration HU and inspiration HU). All matrices were pre-processed to remove any voxels above -500 HU OR below -1000HU, in either inspiration OR expiration HU value. To discuss feature extraction, we use the following notation:

- $L = \{v_i \mid i = 1, \ldots, n\}$, denotes a 'lung set' L, of n voxels v_i.
- $\text{iHU}: L \rightarrow [-1000, -500] \subset \mathbb{Z}$, maps a voxel to its inspiration HU value.
- $\text{eHU}: L \rightarrow [-1000, -500] \subset \mathbb{Z}$, maps a voxel to its expiration HU value.
- $c: L \rightarrow \mathbb{R}^3$, maps a voxel v_i to its Cartesian coordinates (x_i, y_i, z_i).
- $\Delta\text{HU}: L \rightarrow [-500,500] \subset \mathbb{Z}$. $\Delta\text{HU}(v) = \text{eHU}(v) - \text{iHU}(v)$.

All extracted CT features are listed in **Table E1**.

M2.1 *JDH Features*

PRM registered inspiration expiration CT features reported by Galbán et al[E9] were derived from consideration of the inspiration and expiration paired voxel HU distributions. The typical

Gaussian distribution can be well visualized in a joint density histogram; summarizing voxel concentrations in the eHU iHU plane (see **Figure 1 A**). In this study, PRM voxel classification, class: $L \to S \cong \mathbb{Z}_4$, was determined by the following algorithm:

IF [iHU(v) ≥ -950] AND [eHU(v) ≥ -856] THEN [class(v) = PRM^{Norm}]

IF [iHU(v) ≥ -950] AND [eHU(v) < -856] THEN [class(v) = PRM^{fSAD}]

IF [iHU(v) < -950] AND [eHU(v) < -856] THEN [class(v) = PRM^{Emph}]

IF [iHU(v) < -950] AND [eHU(v) ≥ -856] THEN [class(v) = PRM^{Uncl}]

Taking eHU as the horizontal axis, and iHU the vertical, then PRM^{Norm}, PRM^{fSAD}, PRM^{Emph} and PRM^{Uncl} classification relates to the 1st, 2nd, 3rd and 4th quadrants of axes centered at (-856,-950) (see **Figure 1 A** left), and subscripts abbreviate "normal", "functional small airways disease", "emphysema" and "unclassified" respectively. In this study, the features $\%PRM^{s}$ were defined to be the percentage of all voxels classified as PRM^{s}, $s \in \{"Norm", "fSAD", "Emph", "Uncl"\}$. E.g. given a set $\{v_i | i = 1, \dots, n\}$ of n voxels, $\%PRM^{fSAD} = \#\{v_i | class(v_i) = PRM^{fSAD}\}/n$. N.B. percentage has been represented in decimal form for these features.

JDH visualization typically demonstrates an approximate 2-dimensional Gaussian distribution, in which one may perceive an ellipse. The geometrical properties of this ellipse may thus form a means of describing the eHU iHU distribution. In this study, the properties chosen to approximate were minor axis length (ellMinL), major axis length (ellMajL), area (ellArea = $\pi \cdot$ ellMinL $\cdot$ ellMajL) and acute angle between the ellipse and the horizontal (allAngle).

To obtain these properties, the ellipse is first isolated by setting all cells in the JDH, with a voxel count of below $0.25 \cdot$ [maximum cell voxel count], to zero. The co-variance matrix of the resulting voxel count distribution thus provides a description more localized to the ellipse perceived. Eigenvectors of this matrix provide representations of the major and minor axes, and so the area. To calculate ellAngle, the longer Eigenvector is identified (directed along major axis), then if necessary it is negated to obtain vector directed at positive quadrant. Then ellAngle is calculated from using the dot product theorem with the vector (1, 0), i.e. calculating the typically acute angle between the major axis and the horizontal.

M2.2 *Voxel Count (vCnt) Features*

A number of simple features may be defined using voxel amount and ranges.

- $\mathrm{vCnt}(L) = n$, the number of voxels, a measure of total 'lung tissue' volume.
- $\mathrm{vCntX}(L) = \mathrm{range}(\{x_i\})$. $\mathrm{vCntY}(L) = \mathrm{range}(\{y_i\})$. $\mathrm{vCntZ}(L) = \mathrm{range}(\{z_i\})$. Ranges of x, y and z coordinates provide some measure of anterior-posterior, lateral and inferior-superior lung dimensions respectively.

M2.3 *Global ΔHU Features*

ΔHU as defined may be proportional to ventilation in a voxel, and has been previously studied as an immediate quantifier of ventilation behavior[E10, E11, E12]. Mathematical relation between defined PRM voxels classifications and ΔHU function is elucidated in **Figure E5 C**. If a voxel at inspiration contains air, and at expiration has released this air, then the density, reported by HU (associated radiation absorption) should increase, i.e. $\Delta\mathrm{HU} > 0$. It has been seen that this is true for most voxels in all subjects, and $\overline{\Delta\mathrm{HU}} \gg 0$ on average (arithmetic mean). Associations

between $\overline{\Delta HU}^{IS*}$ and weight also lend credence to this assumption[E9], with positive correlation over all subjects of r = 0.51 (2 s.f.) and p < 0.001. It should be noted however that perfusion and imaging artifacts are likely to affect ΔHU and add noise to the ventilation signal.

In statistics, measures of central tendency and spread are two key characteristics that are of immediate interest in any distribution, and so naturally we define:

- $\overline{\Delta HU} : L \to \mathbb{R}$. $\overline{\Delta HU}(L) = \overline{\Delta HU}(L) = \frac{1}{n}\sum_1^n \Delta HU(v_i \in L)$.
- std(ΔHU) : $L \to \mathbb{R}$. $\text{std}(\Delta HU)\,(L) = \sqrt{\frac{\sum_1^n (\Delta HU(v_i) - \overline{\Delta HU})^2}{n-1}}$.

That is the mean and standard deviation (std) of change in HU, intended as a measure of average ventilation and variation in ventilation.

M2.4 *Inter-lung Comparison Features*

Let the voxels belonging to the left lung be the voxel set L_{left}, and likewise for the right lung, L_{right}, such that $L_{\text{left}} \cap L_{\text{right}} = \emptyset$, $L_{\text{left}} \cup L_{\text{right}} = L$. In this study we applied 2-means clustering with centroids initiated at $(\bar{x}, \bar{y} \pm 2\text{std}(y), \bar{z})$, to approximate L_{left} and L_{right} from given data.

Using the ascribed 'ΔHU' functions, we naturally define:

- RLmeanDiff : $L \to \mathbb{R}$, $\text{RLmeanDiff}(L) = \left|\overline{\Delta HU}(L_{\text{left}}) - \overline{\Delta HU}(L_{\text{right}})\right|$.
- RLstdDiff : $L \to \mathbb{R}$, $\text{RLstdDiff}(L) = \left|\text{std}(\Delta HU)\,(L_{\text{left}}) - \text{std}(\Delta HU)\,(L_{\text{right}})\right|$.

That is, measuring the difference in average ventilation, and difference in variation of ventilation, between the two lung voxel sets.

An additional feature is provided through considering the difference in lung sizes, RLsizeRat, read as 'right-left size ratio'. RLsizeRat : $L \to [0,1) \subset \mathbb{R}_{\geq 0}$, $\text{RLsizeRat}(L) = 1 - \min\left\{\frac{vCnt(L_{\text{left}})}{vCnt(L_{\text{right}})}, \frac{vCnt(L_{\text{right}})}{vCnt(L_{\text{left}})}\right\}$. As defined it constitutes a metric (satisfying associated axioms), and is meant to measure extent to which lungs differ in size. A value of 0 can be achieved only if the lungs are equal in size (biologically abnormal), else the value tends to 1 as the difference in lung sizes increases. This feature was found to be associated with R5-R20 (see **Table E4**), indicating a possible role in pulmonary disease.

M2.5 *Stratified Axial Analysis*

Stratified axial analysis (SAA) was developed to provide a basic tool for quantifying ventilation behavior, approximated by ΔHU, as the lung is traversed along a cardinal (x, y or z) axis (see **Figure E1** and **Figure E2**). It works by stratifying the voxels into groups using one of the co-ordinate distributions (x, y or z), then computing a functional average (e.g. $\overline{\Delta \text{HU}}$) for each stratified voxel group individually, and finally presenting a summary of the gradient for this distribution (i.e. on average, how the function changes across the defined strata).

To describe the process in practice, with some operational intricacies, consider *L* the entire set of voxels for a pair of lungs. Then to stratify in the z axis (see **Figure E1 B**), we used the range $= \max(z_i) - \min(z_i)$. A portion of the strata at the poles is eliminated, to reduce noise at the

ends of the distribution of interest. 15% of r, of the extremes, are trimmed, retaining the middle 70% r for the remaining steps. This trimming helps deal with low voxel count at the extremities, difference in lungs heights, and beam hardening effects in the CT image, common to the conical base and apex of the lungs. The remaining voxels are then split into 10 intervals, of roughly 7% r each, with (9) intermediary points termed 'deciles'. One may consider 10 values determined by the function ΔHU on each interval, providing a smoothed indicator of the average 'ventilation' at each level. Then we take the differences at the deciles, with direction chosen to be 'inferior-to-superior' (by ordering in subtraction).

To describe how $\overline{\Delta \mathrm{HU}}$ varies across the intervals, we initially used fitting of a 1 degree polynomial, i.e. straight line, using ordinary least squares (OLS) criterion. The gradient of the resultant line provides a natural measure of change, so we define 4 SAA based attributes as follows:

- $\overline{\Delta \mathrm{HU}}^{\mathbf{AP}}$, gradient measuring $\overline{\Delta \mathrm{HU}}$ change, in the **anterior-posterior** direction.
- $\mathrm{std}(\Delta \mathrm{HU})^{\mathbf{AP}}$, gradient measuring std(ΔHU) change, in the **anterior-posterior** direction.
- $\overline{\Delta \mathrm{HU}}^{\mathbf{IS}}$, gradient measuring$\overline{\Delta \mathrm{HU}}$ change, in the **inferior-superior** direction.
- $\mathrm{std}(\Delta \mathrm{HU})^{\mathbf{IS}}$, gradient measuring std(ΔHU) change, in the **inferior-superior** direction.

Lateral $\overline{\Delta \mathrm{HU}}$ gradient across the lungs was not investigated. As it became clear that inferior-superior ventilation gradient was strongly linked to VH, another method of measuring gradient was applied to this axis, focusing on $\overline{\Delta \mathrm{HU}}$. Termed $\overline{\Delta \mathrm{HU}}^{\mathbf{IS*}}$, this focuses on simply taking the mean of the decile changes (see **Figure E1 B**), as follows:

211

212 • $\overline{\Delta \mathrm{HU}}^{\mathbf{IS*}} = \frac{1}{9}\sum_{1}^{9}\left(\overline{\Delta \mathrm{HU}}(I_{i+1}) - \overline{\Delta \mathrm{HU}}(I_i)\right) = \frac{\overline{\Delta \mathrm{HU}}(I_{10}) - \overline{\Delta \mathrm{HU}}(I_1)}{9}$

213

214 Where I_i is the i[th] interval, travelling from inferior to superior as i ranges from 1 to 10. This
215 happens to be equivalent to a scaled difference between the extreme intervals. This measurement
216 was found to have marginally higher correlational strength, and so possibly a cleaner signal
217 (smoothing measurement to extreme post-trimmed intervals), relative to $\overline{\Delta \mathrm{HU}}^{\mathbf{IS}}$.

218

219 **M3.0 Computational Simulations of Regionalised Bronchoconstriction**

220 Computational calculations of lung impedance were performed through simulation of an
221 electrical-circuit analogous model on patient-specific virtual conducting zone lung structures.
222 Virtual structures were created in a prior study[E14] through processing of inspiratory-expiratory
223 CT scan images. From each scan, centrelines of the central airways (typically up to generation 6)
224 were extracted, and lobar boundaries identified. An algorithmic airway generation process[E11] was
225 used to grow the remainder of the conducting zone (to an average generation of 16) within the
226 defined lobar boundaries.

227

228 Total lung impedance was calculated by assuming each branch had an associated impedance due
229 to oscillatory flow, with each terminal bronchiole being subtended by a viscoelastic acinar unit.
230 The impedance of each individual branch was based off derivations by Benade[E12], and
231 Thurston[E13], with impedance of a branch *j*, experiencing flow at a frequency *f,* given by

$$Z_j = \left(i\,\frac{\omega \rho l}{\pi r_j^2}\right)(1 - F_v e^{i\phi r_j})^{-1},$$

where ρ is air density, $\omega = 2\pi f, l$ and r are the branch length and radius respectively, and $i = \sqrt{-1}$. The exponential contribution is defined as

$$F_v e^{i\phi r_j} = \frac{2}{r_v\sqrt{-i}}\frac{J_1(r_v\sqrt{-i})}{J_0(r_v\sqrt{-i})}, \qquad r_v = \left(\frac{\omega\rho}{\mu}\right)^{1/2} r,$$

where r_v is the boundary layer thickness, μ is the air viscosity, and J_0 and J_1 are the zeroth and first Bessel functions. The viscoelastic acinar units were described by a homogeneous, constant-phase model of the form

$$Z_{acin} = \frac{G - iH}{N\,\omega^{\alpha}},$$

Where G and H are coefficients for tissue damping and elastance respectively (taken as 0.12, and 0.57 kPa.s.L^{-1} [E14]), N is the number of terminal bronchioles, and

$$\alpha = \frac{2}{\pi} tan^{-1}\left(\frac{H}{G}\right).$$

Total impedance of the lung was calculated by adding series and parallel contributions from each acinar region and airway over the entire airway tree. Following the work of Bhatawedakar et al.[E15] this value was then added in series to chest wall, tracheal and glottal resistances and (all taken as 0.049kPa.s.L^{-1}) and chest wall elastances (taken as 1.04kPa.s.L^{-1}), and in parallel to a non-specific shunt impedance.

M4.0 Statistical Analysis

MATLAB R2015a (MATLAB Release 2015a, The MathWorks, Inc., Natick, Massachusetts, United States) was used to perform all statistics and data processing. Results were obtained as output from customized scripts, making use of built-in statistical functions and workflows, for which there is extensive description on the MathWorks website. In all tests with a defined p-value, significance is determined by $p < 0.05$.

M4.1 *Group Comparisons*

Binary group comparisons were performed using built-in function 'kstest' (Kolmogorov-Smirnov), followed by 'ttest2' (two-sample t-test) if attribute determined parametric, and 'ranksum' (equivalent to Mann-Whitney U-test) otherwise. Multiple group comparison (for 3 or more groups) was computed using built-in function 'kstest' (Kolmogorov-Smirnov), followed by 'anova1' (one-way ANOVA) if attribute was determined parametric, and 'kruskalwallis' (Kruskal-Wallis) otherwise. The 'stats' variable from multiple group comparison testing was passed to the 'multcompare' function, with default Tukey's honest significant difference criterion. Output from 'multcompare' was used to define significance in tables. All multiple group comparisons were performed on groups with empty intersections (no overlapping). To compare ratios of a boolean variable across groups, a 3rd party script 'prop_test.m'[1] was utilized to implement a simple two-sample Chi-square test of proportions.

To perform tertile polar analysis, it required, by design, formation of groups with an unnatural distribution (extreme tertiles of a given 'natural' distribution). In this instance, comparisons were performed pairwise on the two groups, across all intervals or deciles, using the 'ranksum' (Wilcoxon Rank-Sum test) function.

M4.2 *Correlation Analysis*

Pearson correlation coefficient was calculated using the 'corrcoef' and 'corr' functions. A script was written to analyze absolute correlation strength above a given threshold, over all pairs of a

[1] https://uk.mathworks.com/matlabcentral/fileexchange/45966-compare-two-proportions--chi-square-?focused=3813016&tab=function

given set of attributes. In cases of missing data, correlation calculation was restricted to subjects for which data was present. Results for attribute pairs above the threshold were presented in terms of scatter plot with graphed line of best fit, and table listing signed correlation coefficient, p-value, and indexes for attributes.

M4.3 *Boxplots*

Box plots and annotations of healthy and asthmatic subjects were created using custom script including 'boxplot' function. In all cases boxplots present differentiation of median split groups for feature included with approximate median value on the horizontal axis. E.g. see **Figure 1 C**. Outliers with respect to split groups are highlighted with black spots (see **Figure E3**).

M4.4 *Tertile Polar Analysis*

Given a suspected signal in noisy data, it can help to focus on attribute extremes. We chose the highest and lowest 16 values from an attribute distribution to compare following this ideology, being approximately distribution tertile poles, since $^{16}/_{52} \approx {}^{1}/_{3}$, chosen to isolate polar behavior whilst preserving numbers for statistical significance. This analysis was applied to relevant attributes to generate groups for comparison in $\overline{\Delta \mathrm{HU}}^{\mathbf{IS*}}$ and $\overline{\Delta \mathrm{HU}}^{\mathbf{AP}}$ interval-wise and decile-wise (used in figures) analysis (see **Figure 3 A** and Figure E4).

M4.5 *Feature and Feature Set Relational Strength Analysis*

In order to determine if two variables, or more generally two sets of variables, are 'related', a well understood and standard approach is to look at linear correlation and discriminatory properties. This approach is limited in the sense that not all relationships may be linear, though

many important relationships between variables in nature are. We utilized correlation and regression modelling to study how CT data, represented by a set of 22 features, relates to various single non-CT attributes, and linear discriminant analysis (LDA) to test relational strength of feature sets to VH discrimination.

M4.6 *Average Correlation*

Given a data matrix $X_{n\times m}$ of m attributes over n subjects, it was desired to see how some submatrix X_s, formed from a selection of columns from X in some order, compares to single attributes from $X\backslash X_s$. Specifically, 22 CT attributes (all that were defined in this study) formed the submatrix X_{CT}, and attributes from spirometry, IOS, MBW and GINA were chosen as target variables. Then average correlation is defined: $\bar{r} = \frac{1}{22}\sum_1^{22}|\mathrm{corr}(x, y)|$, where $x \in X_{CT}$, y is a target variable and 'corr' is the Pearson correlation coefficient over all 52 subjects. This provides one of the simplest though apparently prognostic measures of linear relation. Simple rationale is that if there exists a large number of highly correlating (absolute value) CT variables with a variable y, then y is strongly related (linearly) to 'CT data' (as represented by the given feature set). Results presented in first column of **Table E5**.

M4.7 *Multicollinearity Limited Subset Linear Regression*

Linear regression was utilized to test likelihood (F-statistic) and strength ($R^2 \sim$ variance explained) of linear relation between predictor variables and some outcome variable. In this study we used CT based predictor variables to predict an outcome variable from the aforementioned non-CT attributes. However, the problem of multicollinearity, that is the

existence of strong absolute correlation between input variables begetting ill posed prediction model, should to be handled to reduce likelihood of spurious results.

One method supposed to limit multicollinearity impact, whilst preserving original (un-altered) data values for predictor variables, is to select a 'representative' subset of features, eliminating the occurrence of absolute pairwise correlation above some threshold. An ad hoc approach to feature selection was utilized, whereby data analyst experience and consistency lead decision produced a 14 feature subset (from 22 features) in which no absolute pairwise correlation exceeded 0.7 (see **Figure E2 B**). Specifically: **ellMajL** summarized itself, $\overline{\Delta HU}$ and std(ΔHU); ellMinL summarized itself and ellArea; **RLmeanDiff**, **RLstdDiff** and **RLsizeRat** lacked intra-CT correlation (thus were all included); $\mathbf{PRM^{Emph}}$ summarized PRM_s attributes; **vCntX**, **vCntY** and **vCntZ** all appeared to lack intra-CT correlation, whilst vCnt strongly correlated with vCntZ; All OLS based SAA features, $\overline{\Delta HU}^{\mathbf{AP}}$, $std(\Delta HU)^{\mathbf{AP}}$, $\overline{\Delta HU}^{\mathbf{IS}}$ and $std(\Delta HU)^{\mathbf{IS}}$, lacked intra-CT correlation, and $\overline{\Delta HU}^{\mathbf{IS}}$ was chosen to summarize $\overline{\Delta HU}^{\mathbf{IS*}}$ for consistency. Reader may refer to **Figure E2 A and B** for supporting rationale in these decisions. Results presented in **Table E5**, second column.

M4.8 *PCA Kaiser Rule Linear Regression*

Though given rationality, and the arguably preferable aspect of using original data values, the described multicollinearity limited subset method can be highly sensitive to chosen 'representatives', and loss of information from eliminating attributes. PCA provides another approach to eliminating multicollinearity within data, since by design it produces orthogonal

representative coordinates, principal components, and have correlation strength 0 between any pair of components.

In this study we utilized PCA to provide a low dimensional approximation, by principal components, to X_{CT}. Applying the 'Kaiser rule', we selected the first 6 components, as these had variance explained greater than the average variance explained across all components. These 6 components were then used as predictor variables in linear regression predicting the outcome variables described. Results presented in **Table E5**, third column. One may consider the PCA Kaiser rule (PCA-KR) approach as being a relatively less biased representation of linear strength. Both approaches are presented for consideration.

M4.9 *Linear Discriminant Analysis*

In order to assess 'linear relational strength' between sets of features, representing a more general object (e.g. 'CT data', 'spirometry'), we utilized LDA to determine the best linear discriminator between two sets of points, according to Fisher's criteria of maximal inter-class mean separation with minimal intra-class variance. LDA was implemented using custom MATLAB script, written to show histogram of projected value distribution (see **Figure 5**), and determine classification accuracy from best (least error) one dimensional point of discrimination (see **Table E8**). Coefficients of LDA across all selected features are reported (see **Table E9**).

M4.10 *Joint Density Histogram (JDH) Visualisation*

JDH visualization was generated using the 'surf' function with re-specified tick locations and labels, applied to a 2-dimensional array with dimensions determined by the floor of the range of

the associated distribution (i.e. bin number for binning point counts with respect to a variable set equal to rounded range of that variable). Colormap 'hot' was applied (see **Figure 1 A**) to create black and white compatible presentation. Eigenvectors and Eigenvalues of the 2D array were utilized to determine ellipse axes fitting dual Gaussian distribution (see **Figure 1 A** right), plotted with vectors directed from mean point using square root of associated Eigenvalue to determine length.

M4.11 *Mass Normalised Min-Max Projections*

A simple method to perceive information based on high volume point cloud distribution in 3D is 'min-max projection', that is to project the distribution to some 2D plane, binning 2D cells to count point frequency and visualize using a heatmap; i.e. essentially applying the JDH algorithm just described to some 2D projection of a 3-dimensional distribution. To visualize functional averages in space, replace 'point frequency' with $\sum f(x)$, where x varies over all points in a cell. Then mass bias is cancelled by dividing by number of points in the cell. In this study, such mass normalized min-max projection was applied in the coronal plane to visualize PRM^{fSAD} concentration and $\overline{\Delta HU}$ in high volume voxel clouds (see **Figure 3 B** and **Figure 4**).

RESULTS

R1 *GINA Group Comparisons (Imaging biomarkers of global lung VH are not associated with small airway VH markers R5-R20 and Sacin)*

Binary and non-intersecting multiple group comparisons were performed over all attributes, using algorithms described in *group comparisons*, with subjects grouped according to GINA score, with pairs GINA 2 GINA 3 and GINA 4 GINA 5 pooled due to qualitative treatment

similarity. Specifically, the groups were non-asthmatic (n=11), GINA 1 (n=8), GINA 2 or GINA 3 (n=20), and GINA 4 or GINA 5 (n=13). The results of this analysis are displayed in **Table 1** and **Table E2**; subscripts are used to denote significant differences between groups.

Table 1 reports results across all non-CT features, formatted as mean (± standard deviation) or $[n_1/n_2/\ldots]$ for discrete variables where appropriate. Features are grouped into classes termed 'clinical', 'spirometry', 'MBW' (multiple breath washout), 'IOS' (impulse oscillometry) and 'Sputum'. The same formatting and classification is applied in **Table E3**.

Table E2 reports results across all CT features, formatted as mean (± standard deviation). Features are grouped into classes termed 'PRM' (parametric response map), 'ELL' (ellipse), 'ΔHU' (change in Hounsfield units, between expiration and inspiration), 'ILC' (inter-lung comparison), 'vCNT' (voxel count) and 'SAA' (stratified axial analysis).

R2 *Feature and Feature Set Relational Strength Analysis (Imaging biomarkers of regional VH are major determinants of small airway ventilation VH R5-R20 and Sacin)*

The results of all relational strength analyses are presented in **Table E5**, **Table E6**, **Table E7**, **Table E8**, **Figure 5** and **Figure E6**. Linear statistical analyses were applied to the complete data matrix represented (pairwise absolute correlation strength) in **Figure E6**; these were absolute Pearson's correlation coefficients, multicollinearity reduction through subset selection and PCA, selection of first 6 principal components based on Kaiser rule, and observation of JDH extremes for attribute $FEV_1/FVC(\%)$ which had the strongest (linear association) of all features studied.

Table E5 presents a high level summary of outcomes for linear analyses (non-LDA). 'Corr.' column presents average absolute Pearson's correlation between all CT attributes and listed target attributes (rows). LR (subset) presents R^2 and F-statistic p-values from linear regression, using the described 14 feature subset as predictor variables. LR (PCA) presents the same with principal components 1 through 6 as predictor variables. PCA-LR Coef. (abs. value) presents the loading scores of the principal components in cases were the F-statistic indicted statistically significant ($p < 0.05$) likelihood of a linear relationship, which should be used with **Table E7** for complete interpretation; that is linking principal component loading score magnitude with linear regression co-efficient magnitude to associate CT input features to target non-CT features.

Table E6 presents the coefficients derived in the application of linear regression to the 14 feature subset of CT attributes. Since the coefficient magnitude is dependent on ordering of predictor variables, the values for each input are assessed to determine the largest for a given input variable, and this may then be related to an outcome variable. To give an example, predictor variable with ID 9 (column), which is RLsizeRat (see **Table E7** subscripts), has .44 as its highest magnitude, which belongs to (observe row) outcome variable R5-R20. In fact the outcome variable AX is associated with magnitude .42, significantly higher than all other magnitudes, suggesting association between RLsizeRat and IOS (over other outcome variables). This result may be linked to the observed significance of feature RLsizeRat in **Table E4**; that is it appears as one of the CT variables which discriminates R5-R20 extremes.

Table E7 serves a similar purpose to **Table E6**, though it is dedicated the PCA approach used in linear regression. The loading scores of all 22 CT attributes studied (rows) are presented for all 6

principal components used in the linear regression. Combining this with the final column of **Table E5**, it is possible to study relational strength between outcome and predictor variables. To give an example, R5-R20 has P2 as its highest loading principal component, and observing this column in **Table E7** it is clear that CT feature $\overline{\Delta HU}^{\mathbf{IS*}}$ (practically equivalent to $\overline{\Delta HU}^{\mathbf{IS}}$) has the greatest absolute loading value, suggesting association between $\overline{\Delta HU}^{\mathbf{IS*}}$ and R5-R20. This association, in addition to vCntX (anterior-posterior segmented lung length) and ellMinL, may also be observed in **Table E4**.

R3 *LDA and VH Group Comparisons (Discrimination of Sacin and R5-R20 with imaging markers of density change (ΔHU) gradients and lung size asymmetry)*

LDA results are presented in **Figure 5**, **Table E8** and **Table E9**. Clinical features chosen were age, smoking history [pack years] and weight [kg]. Spirometry features chosen were FEV_1% and FEV_1/FVC(%). CT features chosen were ellMinL, ellArea, std(ΔHU), RLsizeRat, vCntX, vCntZ, $\overline{\Delta HU}^{\mathbf{AP}}$, std(ΔHU)$^{\mathbf{IS}}$ and $\overline{\Delta HU}^{\mathbf{IS}}$ (all features demonstrating VH discrimination in multiple comparison tests). Representative feature sets were chosen following advice from domain expert (clinician).

VH marker mean split groups, R5-R20 low (n=32), R5-R20 high (n=20), S_{acin} low (n=29) and S_{acin} high (n=23), were subjected to standard 1D statistical comparisons. The results are presented in **Table 2** (most prominent for paper), **Table E3** and **Table E4** (extended form of **Table 2**). **Table E3** presents results across all non-CT attributes. **Table E4** presents results across all 22 studied CT features. Features ellMinL, ellArea, std(ΔHU), RLsizeRat, vCntX,

455 vCntZ, $\overline{\Delta HU}^{AP}$, $\overline{\Delta HU}^{IS}$ and $\overline{\Delta HU}^{IS*}$ discriminate R5-R20 extremes. Features std(ΔHU)^{IS}, $\overline{\Delta HU}^{IS}$
456 and $\overline{\Delta HU}^{IS*}$ discriminate S_{acin} extremes.
457
458 $\overline{\Delta HU}^{IS*}$ and $\overline{\Delta HU}^{IS}$ were the **only** features discriminating **both** markers of VH, and $\overline{\Delta HU}^{IS*}$ was
459 found to provide marginally stronger correlations against non-CT features; thus we decided to
460 conduct deeper investigations of $\overline{\Delta HU}^{IS*}$ interaction with VH.
461
462 Correlational, polar and min-max projection analyses were all utilized to study how $\overline{\Delta HU}^{IS*}$
463 relates to non-CT features, to better understand the regionally localized contributions (in inferior-
464 superior strata) to the discrimination of R5-R20 and S_{acin}, and explore possible reasons for the
465 association of inferior-superior ventilation gradient reversal and VH extreme discrimination. The
466 results of this investigative effort are presented in **Figure 3**, **Figure 4** and **Figure E5**.
467
468 Mass normalized min-max projections, in coronal plane, of PRM^{fSAD} and $\overline{\Delta HU}$ in the highest and
469 lowest $\overline{\Delta HU}^{IS*}$ scoring 16 subjects, were observed; the visual results are illustrated in **Figure 4**.
470 A number of subjects with high $\overline{\Delta HU}^{IS*}$ appear to have a heterogeneous, and basally focused,
471 distribution of disease markers, with apically preferential ventilation distribution, relative to the
472 more homogeneous distributions observed in subjects with low $\overline{\Delta HU}^{IS*}$. A phenotypical
473 suggestion arising from this observation is summarized in **Figure 4 D**.

References

E1. Oostveen E, MacLeod D, Lorino H, Farre R, Hantos Z, Desager K, et al. The forced oscillation technique in clinical practice: methodology, recommendations and future developments. Eur Respir J. 2003 Dec 1;22(6):1026-41.

E2. Robinson P, Latzin P, Verbanck S, Hall G, Horsley A, Gappa M, et al. Consensus statement for inert gas washout measurement using multiple-and singlebreath tests. Eur Respir J. 2013;41(3):507-22.

E3. Horsley AR, Gustafsson PM, Macleod KA, Saunders C, Greening AP, Porteous DJ, et al. Lung clearance index is a sensitive, repeatable and practical measure of airways disease in adults with cystic fibrosis. Thorax. 2008 Feb 1;63(2):135-40.

E4. Robinson PD, Goldman MD, Gustafsson PM. Inert gas washout: theoretical background and clinical utility in respiratory disease. Respiration. 2009;78(3):339-55.

E5. Galbán CJ, Han MK, Boes JL, Chughtai KA, Meyer CR, Johnson TD, et al. Computed tomography-based biomarker provides unique signature for diagnosis of COPD phenotypes and disease progression. Nat Med. 2012 Nov 1;18(11):1711-5.

E6. Lee SM, Seo JB, Kim N, Oh SY, Oh YM. Optimal threshold of subtraction method for quantification of air-trapping on coregistered CT in COPD patients. Eur Radiol. 2016 Jul 1;26(7):2184-92.

E7. Pennati F, Salito C, Baroni G, Woods J, Aliverti A. Comparison between multivolume CT-based surrogates of regional ventilation in healthy subjects. Acad Radiol. 2014 Oct 31;21(10):1268-75.

E8. Choi S, Hoffman EA, Wenzel SE, Tawhai MH, Yin Y, Castro M, et al. Registration-based assessment of regional lung function via volumetric CT images of normal subjects vs. severe asthmatics. J Appl Physiol. 2013 Sep 1;115(5):730-42.

E9. Holley HS, Milic-Emili J, Becklake MR, Bates DV. Regional distribution of pulmonary ventilation and perfusion in obesity. J Clin Investig. 1967 Apr;46(4):475.

E10. Bordas R, Lefevre C, Veeckmans B, Pitt-Francis J, Fetita C, Brightling CE, et al. Development and analysis of patient-based complete conducting airways models. PLOS ONE. 2015 Dec 11;10(12):e0144105.

E11. Tawhai MH, Hunter P, Tschirren J, Reinhardt J, McLennan G, Hoffman EA. CT-based geometry analysis and finite element models of the human and ovine bronchial tree. J Appl Physiol. 2004 Dec 1;97(6):2310-21.

E12. Benade AH. On the propagation of sound waves in a cylindrical conduit. J Acoust Soc Am. 44(2): 616-623, 1968.

E13. Thurston GB. Periodic fluid flow through circular tubes. J Acoust Soc Am. 24(6): 653-656, 1952.

E14. Kaczka DW, Ingenito EP, Suki B, Lutchen KR. Partitioning airway and lung tissue resistances in humans: effects of bronchoconstriction. J Appl Physiol. 1997 May 1;82(5):1531-41.

E15. Bhatawadekar SA, Leary D, Maksym GN. Modelling resistance and reactance with heterogeneous airway narrowing in mild to severe asthma. Can J Physiol Pharmacol. 2015 Jan 21;93(3):207-14.

516 **Table E1.** Reference list describing extracted CT attributes investigated in this study.

CT Feature	Description
$\overline{\Delta HU}$	Average ΔHU over all segmented voxels.
std(ΔHU)	Standard deviation of ΔHU over all segmented voxels.
ellMajL	Length of major axis, of ellipse perceived in JDH.
ellMinL	Length of minor axis, of ellipse perceived in JDH.
ellArea	Area of ellipse perceived in JDH.
ellAngle	Angle (radians) between major axis and horizontal, of ellipse perceived in JDH.
RLmeanDiff	Absolute difference of average ΔHU between the two lungs.
RLstdDiff	Absolute difference of standard deviation in ΔHU between the two lungs.
RLsizeRat	Ratio of lung voxel counts (two lungs), with larger count in the denominator.
$\%PRM^{Norm}$	Percentage of voxels classified as PRM^{Norm}.
$\%PRM^{fSAD}$	Percentage of voxels classified as PRM^{fSAD}.
$\%PRM^{Emph}$	Percentage of voxels classified as PRM^{Emph}.
$\%PRM^{Uncl}$	Percentage of voxels classified as PRM^{Uncl}.
vCnt	Total voxel count (segmented voxel set).
vCntX	Maximum difference in voxel x-coordinates (anterior-posterior measure).
vCntY	Maximum difference in voxel y-coordinates (lateral measure).
vCntZ	Maximum difference in voxel z-coordinates (inferior-superior measure).
$std(\Delta HU)^{\mathbf{AP}}$	Gradient of ΔHU standard deviation variability in anterior-posterior direction.
$\overline{\Delta HU}^{\mathbf{AP}}$	Gradient of ΔHU mean variability in anterior-posterior direction.
$std(\Delta HU)^{\mathbf{IS}}$	Gradient of ΔHU standard deviation variability in inferior-superior direction.
$\overline{\Delta HU}^{\mathbf{IS}}$	Gradient of ΔHU mean variability in inferior-superior direction.
$\overline{\Delta HU}^{\mathbf{IS*}}$	Difference of ΔHU mean in extreme deciles, in inferior-superior direction.

517
518 HU, Hounsfield Unit; SAA, Stratified Axial Analysis; fSAD, functional small airways disease;
519
520 Basic descriptions of all 22 CT features considered in this study. Intended reading of names is as follows: $\overline{\Delta HU}$ =
521 average ΔHU, std(ΔHU) = ΔHU standard deviation, ellMajL = ellipse major length, ellMinL = ellipse minor length,
522 ellArea = ellipse area, ellAngle = ellipse angle, RLmeanDiff = right-left mean difference, RLstdDiff = right-left
523 standard deviation difference, RLsizeRat = right-left size ratio, $\%PRM^{Norm}$ = percent PRM normal, $\%PRM^{fSAD}$ =
524 percent PRM fSAD, $\%PRM^{Emph}$ = percent PRM emphysema, $\%PRM^{Uncl}$ = percent PRM unclassified, vCnt = voxel
525 count, vCntX = voxel count in x-direction (likewise for vCntY, vCntZ), $std(\Delta HU)^{\mathbf{AP}}$ = 1st degree polynomial fitting

526 to standard deviation in x direction (an SAA based measure, likewise for std(ΔHU)$^{\mathbf{IS}}$), $\overline{\Delta \mathrm{HU}}^{\mathbf{AP}}$ = as std(ΔHU)$^{\mathbf{AP}}$ with
527 averages (likewise for $\overline{\Delta \mathrm{HU}}^{\mathbf{IS}}$), $\overline{\Delta \mathrm{HU}}^{\mathbf{IS*}}$ = extreme difference in inferior-superior direction.
528

Table E2. CT data across all groups, with treatment rationalized GINA stratification applied to asthma cohort.

		Asthma			
	Control (n=11)	**All** (n=41)	**GINA 1** (n=8)	**GINA 2/3** (n=20)	**GINA 4/5** (n=13)
PRM					
$\%PRM^{Norm}$	0.74 (± 0.08)	0.72 (± 0.13)	0.69 (± 0.20)	0.72 (± 0.12)	0.75 (± 0.10)
$\%PRM^{fSAD}$	0.16 (± 0.08)	0.20 (± 0.11)	0.23 (± 0.17)	0.20 (± 0.09)	0.17 (± 0.10)
$\%PRM^{Emph}$	0.028 (± 0.018)	0.031 (± 0.031)	0.039 (± 0.040)	0.033 (± 0.034)	0.023 (± 0.019)
$\%PRM^{Uncl}$	$0.072\ (\pm\ 0.029)_A$	$0.049\ (\pm\ 0.034)_H$	0.041 (± 0.035)	0.045 (± 0.032)	0.058 (± 0.037)
ELL					
ellMajL	$144.4\ (\pm\ 30.0)_A$	$123.5\ (\pm\ 27.8)_H$	118.1 (± 33.2)	122.6 (± 28.8)	128.4 (± 24.0)
ellMinL	55.3 (± 10.0)	55.8 (± 10.6)	53.4 (± 10.9)	56.1 (± 12.2)	56.8 (± 8.1)
ellArea	6411 (± 2375)	5556 (± 2060)	5131 (± 2282)	5597 (± 2381)	5755 (± 1401)
ellAngle	$0.13\ (\pm\ 0.07)_A$	$0.21\ (\pm\ 0.18)_H$	0.25 (± 0.16)	0.21 (± 0.09)	0.18 (± 0.12)
ΔHU					
$\overline{\mathbf{\Delta HU}}$	125.98 (± 39.18)	98.16 (± 42.85)	94.70 (± 63.85)	92.12 (± 27.06)	109.60 (± 48.71)
std(**ΔHU**)	$112.58\ (\pm\ 12.01)_A$	$102.83\ (\pm\ 13.30)_H$	97.77 (± 17.29)	102.11 (± 13.60)	107.04 (± 9.21)
ILC					
RLmeanDiff	11.33 (± 8.64)	10.42 (± 9.91)	10.05 (± 8.49)	9.46 (± 8.15)	12.13 (± 13.25)
RlstdDiff	4.74 (± 5.24)	4.70 (± 3.53)	4.89 (± 3.70)	4.98 (± 4.00)	4.15 (± 2.79)
RlsizeRat	0.198 (± 0.074)	0.170 (± 0.091)	0.177 (± 0.043)	0.159 (± 0.077)	0.183 (± 0.129)
vCNT					
vCnt†	8.23 (± 2.07)	8.76 (± 2.93)	8.81 (± 3.31)	8.66 (± 2.93)	8.87 (± 2.91)
vCntX	240.6 (± 23.3)	234.5 (± 31.5)	232.9 (± 13.9)	235.8 (± 35.8)	233.6 (± 33.9)
vCntY	343.5 (± 22.0)	335.3 (± 25.9)	327.3 (± 20.5)	$327.7\ (\pm\ 24.6)_3$	$351.8\ (\pm\ 24.4)_2$
vCntZ	436.0 (± 41.7)	439.9 (± 50.2)	449.3 (± 70.0)	442.3 (± 46.7)	430.5 (± 43.9)
SAA					
$\text{std}(\Delta HU)^{\mathbf{AP}}$	0.078 (± 0.070)	0.061 (± 0.069)	0.038 (± 0.066)	0.070 (± 0.070)	0.063 (± 0.071)
$\overline{\mathbf{\Delta HU}}^{\mathbf{AP}}$	$0.580\ (\pm\ 0.182)_A$	$0.432\ (\pm\ 0.217)_H$	0.470 (± 0.223)	0.397 (± 0.211)	0.462 (± 0.232)
$\text{std}(\Delta HU)^{\mathbf{IS}}$	-0.071 (± 0.046)	-0.061 (± 0.041)	-0.073 (± 0.043)	-0.062 (± 0.044)	-0.053 (± 0.037)
$\overline{\mathbf{\Delta HU}}^{\mathbf{IS}}$	-0.023 (± 0.159)	-0.013 (± 0.095)	-0.084 (± 0.083)	0.003 (± 0.098)	0.008 (± 0.083)
$\overline{\mathbf{\Delta HU}}^{\mathbf{IS*}}$	-1.460 (± 6.312)	-0.772 (± 3.725)	-2.835 (± 3.085)	-0.488 (± 4.199)	0.061 (± 3.008)

PRM, Parametric Response Map; ELL, ELLipse measurements; HU, Hounsfield Unit; ILC, Inter Lung Comparison; vCNT, voxel count; SAA, Stratified Axial Analysis.

Data expressed as mean (± standard deviation). Attribute normality was tested using one-sample Kolmogorov-Smirnov test over all subjects. Binary group comparisons ('control' vs 'all) were performed using two sample t-test for parametric variables, and Mann-Whitney U-test for non-parametric variables. Non-intersecting multiple group comparisons were performed using one-way ANOVA for parametric variables, and Kruskal-Wallis test for non-parametric variables. Multiple-comparison procedures were performed with Turkey's honest significant difference criterion. Groups with significant separation ($p < 0.05$) indicated by subscripts A (all asthma), H (healthy control), 1, 2, 3 (GINA 1, 2/3 and 4/5 respectively) and * (all other groups).

Table E3. Non-CT features with ventilation heterogeneity based stratification.

	S_{acin}		R5-R20	
	Low (n=29)	**High** (n=23)	**Low** (n=32)	**High** (n=20)
Clinical				
GINA [H/1/2/3/4/5]	[9/5/0/8/5/2]	[2/3/3/9/5/1]	[8/6/1/10/6/1]	[3/2/2/7/4/2]
Age	50.7 (± 12.9)	57.6 (± 11.9)	52.0 (± 12.3)	56.6 (± 13.5)
Sex [M/F]	[12/17]	[12/11]	[13/19]	[11/9]
Weight (kg) †	79.0 (± 20.0)	76.8 (± 13.1)	72.9 (± 15.4)	86.3 (± 17.0)
Height (cm)	168.5 (± 11.2)	166.3 (± 9.7)	166.6 (± 11.2)	169.0 (± 9.6)
BMI†	27.6 (± 5.3)	27.3 (± 4.4)	26.2 (± 4.2)	29.5 (± 5.2)
Atopy [Yes/No]	[16/13]	[17/6]	[22/12]	[11/9]
Pack Years†	6.25 (± 18.45)	7.15 (± 10.98)	2.85 (± 5.76)	12.71 (± 22.91)
No. of Ex. (past yr)	1.1 (± 1.7)	1.0 (± 2.2)	1.0 (± 1.8)	1.2 (± 2.2)
Asthma Duration	15.4 (± 15.8)	19.7 (± 17.7)	18.9 (± 15.8)	15.8 (± 18.2)
Equiv. CS Dose	875.0 (± 779.3)	766.7 (± 625.6)	812.5 (± 726.1)	829.4 (± 678.0)
Spirometry				
FEV_1% *,†	108.2 (± 17.2)	92.6 (± 22.6)	107.5 (± 19.9)	91.4 (± 19.6)
FEV_1/FVC(%)*	79.3 (± 5.2)	71.1 (± 12.6)	77.1 (± 6.8)	73.3 (± 13.6)
Pre-BD FEV_1(L)*, †	3.03 (± 0.90)	2.23 (± 0.78)	2.92 (± 0.94)	2.28 (± 0.79)
Post-BD FEV_1(L)*, †	3.19 (± 0.91)	2.56 (± 0.79)	3.10 (± 0.93)	2.60 (± 0.80)
%BD+/-*	5.99 (± 9.2)	17.13 (± 18.48)	7.36 (± 9.93)	16.60 (± 19.75)
MBW				
LCI*,†	7.17 (± 0.91)	8.37 (± 1.28)	7.40 (± 1.04)	8.17 (± 1.39)
S_{acin}*	0.118 (± 0.039)	0.282 (± 0.102)	0.176 (± 0.097)	0.214 (± 0.126)
S_{cond}	0.032 (± 0.026)	0.040 (± 0.025)	0.038 (± 0.026)	0.030 (± 0.026)
IOS				
R5-R20†	0.043 (± 0.045)	0.070 (± 0.062)	0.025 (± 0.021)	0.103 (± 0.057)
AX†	0.414 (± 0.372)	0.757 (± 0.923)	0.278 (± 0.169)	1.025 (± 0.929)
Sputum				
Eos	0.294 (± 1.443)	0.788 (± 1.896)	0.385 (± 1.525)	0.714 (± 1.867)
Neut	56.10 (± 25.73)	59.22 (± 21.55)	58.50 (± 23.60)	56.23 (± 24.34)

M, male; F, female; BMI, body mass index; FEV, forced expiratory volume; FVC, forced vital capacity; BD, bronchodilator; LCI, lung clearance index; AX, area of reactance; Eos, eosinophil count; Neut, neutrophil count.

Data expressed as mean (± standard deviation). Attribute normality was tested using one-sample Kolmogorov-Smirnov test over all subjects. Binary group (i.e. S_{acin} low vs. S_{acin} high, and R5-R20 low vs. R5-R20 high) comparisons were performed using two sample t-test for parametric variables, and Mann-Whitney U-test for non-parametric variables. Groups with significant separation ($p < 0.05$) of S_{acin} (R5-R20) indicated by * (†).

549 **Table E4.** Computed tomography imaging biomarkers and ventilation heterogeneity based stratification (full).

	S_{acin}		R5-R20	
	Low (n=29)	**High** (n=23)	**Low** (n=32)	**High** (n=20)
PRM				
$\%PRM^{Norm}$	0.74 (± 0.11)	0.71 (± 0.14)	0.72 (± 0.14)	0.73 (± 0.09)
$\%PRM^{fSAD}$	0.19 (± 0.10)	0.19 (± 0.12)	0.19 (± 0.12)	0.18 (± 0.08)
$\%PRM^{Emph}$	0.024 (± 0.018)	0.038 (± 0.037)	0.032 (± 0.033)	0.028 (± 0.021)
$\%PRM^{Uncl}$	0.046 (± 0.036)	0.063 (± 0.030)	0.053 (± 0.038)	0.055 (± 0.028)
ELL				
ellMajL	126.2 (± 30.0)	130.2 (± 28.9)	122.0 (± 28.3)	137.5 (± 29.0)
ellMinL †	55.1 (± 9.4)	56.5 (± 11.8)	52.1 (± 9.1)	61.4 (± 10.0)
ellArea †	5590 (± 2067)	5922 (± 2251)	5092 (± 1763)	6769 (± 2312)
ellAngle	0.21 (± 0.13)	0.16 (± 0.09)	0.19 (± 0.11)	0.20 (± 0.11)
ΔHU				
$\overline{\Delta \mathbf{HU}}$	100.42 (± 48.02)	108.62 (± 36.97)	103.69 (± 45.02)	104.62 (± 41.46)
std(**ΔHU**) †	102.37 (± 14.32)	108.07 (± 12.01)	101.74 (± 12.55)	109.93 (± 13.81)
ILC				
RLmeanDiff	8.48 (± 9.37)	13.30 (± 9.36)	11.05 (± 10.38)	9.91 (± 8.36)
RLstdDiff	4.15 (± 3.94)	5.40 (± 3.81)	5.53 (± 4.33)	3.39 (± 2.68)
RLsizeRat †	0.184 (± 0.088)	0.166 (± 0.088)	0.201 (± 0.087)	0.135 (± 0.073)
vCnt				
vCnt ¥	8.67 (± 2.99)	8.62 (± 2.51)	8.97 (± 2.80)	8.12 (± 2.68)
vCntX †	231.9 (± 25.3)	240.7 (± 34.7)	225.9 (± 27.1)	251.7 (± 27.6)
vCntY	336.9 (± 27.5)	337.2 (± 22.4)	335.8 (± 25.3)	338.9 (± 25.4)
vCntZ †	438.4 (± 45.7)	439.9 (± 52.1)	451.3 (± 48.4)	419.5 (± 41.9)
SAA				
$\text{std}(\Delta HU)^{\mathbf{AP}}$	0.070 (± 0.078)	0.059 (± 0.057)	0.055 (± 0.068)	0.080 (± 0.070)
$\overline{\Delta \mathbf{HU}}^{\mathbf{AP}}$ †	0.473 (± 0.207)	0.450 (± 0.234)	0.512 (± 0.226)	0.386 (± 0.183)
$\text{std}(\Delta HU)^{\mathbf{IS}}$	-0.077 (± 0.043)	-0.046 (± 0.035)	-0.064 (± 0.040)	-0.062 (± 0.047)
$\overline{\Delta \mathbf{HU}}^{\mathbf{IS}}$ *,†	-0.043 (± 0.112)	0.021 (± 0.099)	-0.051 (± 0.100)	0.044 (± 0.102)
$\overline{\Delta \mathbf{HU}}^{\mathbf{IS*}}$ *,†	-2.033 (± 4.372)	0.489 (± 3.936)	-2.282 (± 4.018)	1.267 (± 3.987)

550 ¥ values expressed have multiplier 10^6.

551

552 PRM, Parametric Response Map; ELL, Ellipse measurements; HU, Hounsfield Unit; ILC, Inter Lung Comparison;
553 vCNT, voxel count; SAA, Stratified Axial Analysis.

554

555 Data expressed as mean (± standard deviation). Attribute normality was tested using one-sample Kolmogorov-
556 Smirnov test over all subjects. Binary group (i.e. S_{acin} low vs. S_{acin} high, and R5-R20 low vs. R5-R20 high)
557 comparisons were performed using two sample t-test for parametric variables, and Mann-Whitney U-test for non-
558 parametric variables. Groups with significant separation ($p < 0.05$) of S_{acin} (R5-R20) indicated by * (†).

559 **Table E5.** Summary of linear statistical analyses: average correlation and linear regression (raw value & PCA).

	Corr.	LR (subset)		LR (PCA)		PCA-LR Coef. (abs. value)					
Attribute ID	$\bar{r}$	R^2	**p**	R^2	**p**	**P1**	**P2**	**P3**	**P4**	**P5**	**P6**
FEV_1% 23	.158	.45	p < .05	.19	p > .5	-	-	-	-	-	-
FEV_1/FVC(%) 24	.244	.63	p < .001	.34	p < .005	.37	.19	**.40**	.09	.08	.00
Pre-BD FEV_1 25	.141	.61	p < .001	.29	p < .05	.12	.16	.10	.21	.08	**.44**
Post-BD FEV_1 26	.133	.59	p < .001	.31	p < .05	.09	.10	.10	.30	.15	**.42**
%BD+/- 27	.133	.41	p < .05	.16	p > .05	-	-	-	-	-	-
R5-R20 28	.203	.59	p < .001	.29	p < .05	.00	**.52**	.07	.09	.07	.01
AX 29	.166	.51	p < .05	.19	p > .05	-	-	-	-	-	-
LCI 30	.133	.53	p < .05	.19	p > .05	-	-	-	-	-	-
S_{cond} 31	.132	.24	p > .05	.08	p > .5	-	-	-	-	-	-
S_{acin} 32	.159	.52	p < .05	.28	p < .05	.12	.15	**.42**	.09	.09	.22
GINA 33	0.103	0.46	p < .05	.12	p > .05	-	-	-	-	-	-

560
561 FEV, Forced Expiratory Volume; FVC, Forced Vital Capacity; BD, Bronchodilator; AX, Area of Reactance; LCI,
562 Lung Clearance Index; GINA, Global Initiative for Asthma;
563
564 Single feature CT linear statistical analysis overview. $\bar{r}$ = Pearson's correlation coefficient; R^2 = prediction strength
565 as variance explained; p = p-value from F statistic (test likelihood of significant linear relationship); P1 – P6 =
566 principal components selected by Kaiser rule (above mean variance explained in PCA), in order of variance
567 explained. Corr. (correlation) column illustrates average correlation as crude measure of relation. LR columns (3, 4,
568 5 and 6) represent linear regression outcome using 14 feature subset and PCA principal components as predictor
569 variables, and non-CT (first column) attributes as target variables. Final columns (7… 12) are absolute values of
570 coefficients in linear regression model for PCA, used with table E7 to infer connection between target variables and
571 CT features. Coefficients for 14 feature linear regression are listed in table E6.

572 **Table E6.** Linear regression co-efficient table for linearity reduced CT subset regressions.

		LR Coefficients (absolute value) **by Correlation Matrix** (see Figure E6) **ID**												
		3	4	7	8	9	12	15	16	17	18	19	20	21
LR Target Variable	FEV_1%	.97	.49	.14	.07	.04	.22	.28	.02	.48	.07	.06	**.63**	.23
	FEV_1/FVC(%)	1.4	.64	.29	**.28**	.02	.31	.23	.13	.35	.13	.49	.55	.02
	Pre-BD FEV_1	**1.5**	.80	.38	.10	.17	.02	.14	.45	.60	.21	.41	.45	.11
	Post-BD FEV_1	1.4	.72	.35	.05	.11	.04	.15	**.48**	**.61**	.22	.46	.32	.18
	%BD+/-	.80	.57	.29	.23	.29	.05	.13	.07	.21	.18	.06	.59	.22
	R5-R20	.80	.83	.41	.04	**.44**	.09	.26	.02	.21	.03	.59	.03	.28
	AX	1.0	.89	.43	.16	.42	.15	.16	.09	.19	.08	**.71**	.12	.27
	LCI	1.1	**1.1**	.05	.05	.21	.15	.15	.14	.05	.06	.11	.36	.51
	S_{acin}	.98	.95	**.49**	.07	.12	.23	.03	.13	.33	.01	.64	.20	**.53**
	GINA	1.2	.41	.41	.21	.10	**.37**	**.42**	.19	.27	**.28**	.11	.49	.28

573
574 LR, Linear Regression; FEV, Forced Expiratory Volume; FVC, Forced Vital Capacity; BD, Bronchodilator; AX,
575 Area of Reactance; LCI, Lung Clearance Index; GINA, Global Initiative for Asthma.
576
577 Absolute value of linear regression coefficients over all 14 features selected for raw value linear regression. Refer to
578 table E7 for linking ID numbers (heading row) to CT features. Each predictor feature (column) has highest occurring
579 value in bold. Relational strength between individual predictor and target variables may be assessed through cross-
580 referencing cell co-ordinates with relative co-efficient magnitude for a given feature.

Table E7. Principal component loading scores for components used in linear regression.

	Attribute $_{ID}$	PC1	PC2	PC3	PC4	PC5	PC6
ΔHU	$\overline{\Delta HU}_{1}$	**+.31**	-.11	+.17	-.03	-.17	+.15
	std(ΔHU) $_{2}$	+**.31**	+.10	+.13	+.19	+.08	+.11
ELL	ellMajL $_{3}$	+**.33**	+.09	-.01	+.06	+.12	+.06
	ellMinL $_{4}$	+.17	**+.33**	-.24	-.01	+.17	+.04
	ellArea $_{5}$	+.27	+.23	-.12	+.05	+.16	+.03
	ellAngle $_{6}$	-.25	+.09	**-.30**	-.12	+.15	-.07
ILC	RLmeanDiff $_{7}$	+.17	-.21	+.12	-.21	+**.34**	-.15
	RLstdDiff $_{8}$	-.05	-.19	+.04	-.24	+**.63**	-.04
	RLsizeRat $_{9}$	+.12	-.25	-.00	-.19	+.34	+.00
PRM	$\%PRM^{Norm}{}_{10}$	+.27	-.02	-.29	-.24	-.15	+.10
	$\%PRM^{fSAD}{}_{11}$	**-.32**	+.05	+.08	+.17	+.15	-.16
	$\%PRM^{Emph}{}_{12}$	-.19	+.01	**+.42**	+.23	+.11	-.07
	$\%PRM^{Uncl}{}_{13}$	+.18	-.10	**+.44**	+.13	-.03	+.18
vCNT	vCnt $_{14}$	-.29	+.05	+.17	-.28	-.08	+.17
	vCntX $_{15}$	-.06	**+.35**	+.14	-.22	-.01	+.27
	vCntY $_{16}$	-.07	+.22	+.11	**-.40**	+.08	**+.56**
	vCntZ $_{17}$	-.25	-.12	+.19	-.25	-.15	+.06
SAA	$std(\Delta HU)^{AP}{}_{18}$	-.14	+.16	+.04	**+.41**	**+.34**	**+.32**
	$\overline{\Delta HU}^{AP}{}_{19}$	+.13	**-.36**	+.14	+.14	-.03	+.26
	$std(\Delta HU)^{IS}{}_{20}$	+.19	+.03	**+.30**	**-.35**	-.09	**-.37**
	$\overline{\Delta HU}^{IS}{}_{21}$	+.07	**+.38**	+.23	-.00	+.06	-.27
	$\overline{\Delta HU}^{IS*}{}_{22}$	+.09	**+.38**	+.23	-.07	+.04	-.24

PC, Principal Component; PRM, Parametric Response Map; ELL, Ellipse measurements; HU, Hounsfield Unit; ILC, Inter Lung Comparison; vCNT, voxel count; SAA, Stratified Axial Analysis.

Signed loading scores in PCA over all 22 CT features, as they load onto the first 6 principal components submitted to linear regression in linear statistical analyses. Magnitudes may be considered indicative of feature (row) relational strength to principal component (column) formation, which in turn may be associatively connected to predicted variables (see table E5 far right column).

Table E8. Linear discriminant analysis based classification percentage accuracy with selected feature sets.

	S_{acin} (% accuracy)	**R5-R20** (% accuracy)
Clinical characteristics	63	77
Post BD spirometry	73	69
CT biomarkers	79	83
Clinical + Spirometry	75	77
Clinical + CT	81	87
Spirometry + CT	79	85
Clinical + Spirometry + CT	85	85

LEGEND: Data expressed as percentage of subjects correctly classified by best possible linear discriminant from linear discriminant analysis. Feature sets use attributes representing clinical (age, smoking history [pack years] and weight [kg]), spirometry (FEV_1% and FEV_1/FVC(%)) and CT (ellMinL, ellArea, std(ΔHU), RLsizeRat, vCntX, vCntZ, $\overline{\Delta HU}^{\mathbf{AP}}$, std(ΔHU)$^{\mathbf{IS}}$ and $\overline{\Delta HU}^{\mathbf{IS}}$ [features differentiating S_{acin} **or** R5-R20]) data.

602 **Table E9.** Linear discriminant analysis coefficients on combined feature sets.

603

	S_{acin}	R5-R20
Clinical characteristics		
Age (completed years)	-0.014	+0.010
Weight (kg)	**+0.028**$^{▼}$	+0.014
Smoking (pack years)	-0.0060	-0.016
Post BD spirometry		
FEV_1%	+0.017	+0.022
FEV_1/FVC(%)	+0.014	+0.013
CT biomarkers		
std(ΔHU)	-0.021	+0.0056
ellMinL	+0.012	**+0.044**$^{▼}$
ellArea	**-0.032**$^{▲}$	**-0.080**$^{▲}$
RLsizeRat	-0.00040	+0.014
vCntX	-0.00073	-0.015
vCntZ	-0.022	+0.0047
$\overline{\Delta HU}^{\mathbf{AP}}$	+0.0069	-0.00054
std(ΔHU)$^{\mathbf{IS}}$	-0.011	+0.028
$\overline{\Delta HU}^{\mathbf{IS}}$	-0.0020	-0.022

604
605
606 LEGEND: Coefficients of linear discriminant analysis (LDA) applied across all selected features. S_{acin} or
607 R5-R20 below mean groups are projected in positive direction. Above mean groups are projected in
608 negative direction. Thus more positive coefficients may be associated with less ventilation heterogeneity
609 (VH), and more negative coefficients with more VH. Extremes of greatest magnitude are emphasised in
610 **bold**. Superscript ▲ indicates most associated with **high VH** (relatively most negative
611 coefficient), and ▼ with **low VH** (relatively most positive coefficient).

Figure legends

Figure E1. ΔHU derivation and inferior-superior SAA technical illustration. A, rationale behind assumption that simple change in HU (from inspiration to expiration), approximately change in local volume, is associated with ventilation / gas release. B, exemplar demonstration of SAA applied to the inferior-superior axis, and precise definition of $\overline{\Delta HU}^{IS*}$, notably being a scaled (1/9) difference in average HU between polar voxel intervals.

Figure E2. Decile based ΔHU gradient measures and combinatorial voxel features. A, inferior-to-superior (anterior-to-posterior) stratification of lungs, with 15% (10%) of range trimmed at ends; $\overline{\Delta HU}^{IS*}$ calculated as difference of extreme (shaded) strata. B, combinatorial features, based on coordinate axis ranges and voxel counts between segmented left and right lungs (lung asymmetry); subject illustrated chosen for clear case of visual asymmetry.

Figure E3. Box plot illustration of ellipse area and $\%PRM^{fSAD}$ association with VH markers S_{acin} and R5-R20; groups formed about median value of VH markers. Apparent lack of group separation relative to splitting on median FEV1/FVC% (figure 1).

Figure E4. Anterior-to-posterior VH marker focused polar analysis. SAA deciles plotted as mean and standard deviation (bar lengths) of HU changes, highlighting significant regions related to both S_{acin} and R5-R20.

Figure E5. Comparison of ΔHU in PRM^{x} voxel populations, in $\overline{\Delta HU}^{IS*}$ low and high tertile, and illustration of relationship between ΔHU and PRM^{x} on exemplar JDH. A, $\overline{\Delta HU}^{IS*}$ low tertile boxplots of ΔHU by PRMx class. B, $\overline{\Delta HU}^{IS*}$ high tertile boxplots of ΔHU by PRM^{x} class. Variance appears reduced in B relative to A (common observation: disease brings pressure to biological system, leading to reduced variance). C, illustration of ΔHU projection overlaid onto an exemplar JDH (same case as panel A in Figure 1). Essentially it is a projection (x,y) in 2D onto x-y in 1D. Line of no change (x=y) plotted in green, and relayed over boxplot figures in A and B. Reader should be able to appreciate reason for ordering of boxplots in A and B, e.g. PRM^{Uncl} has highest ΔHU, as this quadrant of the JDH lies furthest in the positive ΔHU direction (similar reasoning can be used for PRM^{fSAD}).

640 **Figure E6.** Complete original data matrix correlation visualization and reduction technique. A, illustration of
641 absolute correlation matrix, annotated with feature set nomenclature, and indicating features selected for raw value
642 linear regression. B, pairwise-correlation visualization and collinearity reduction.

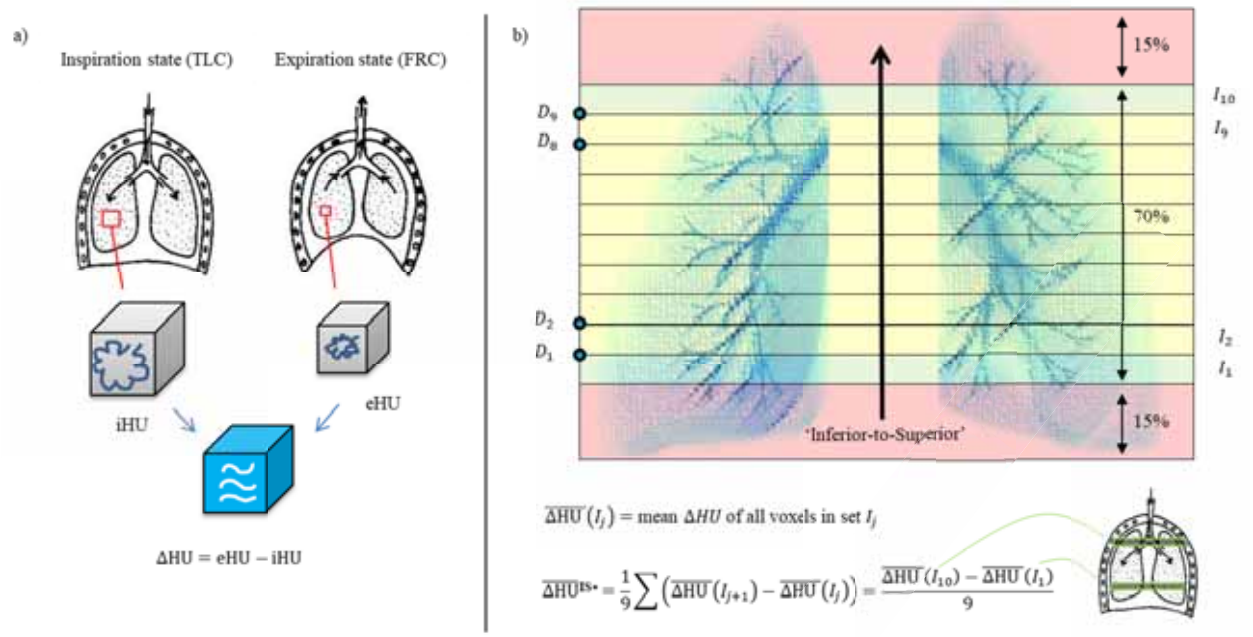

a) Regional PRM, measuring gradients of ΔHU.

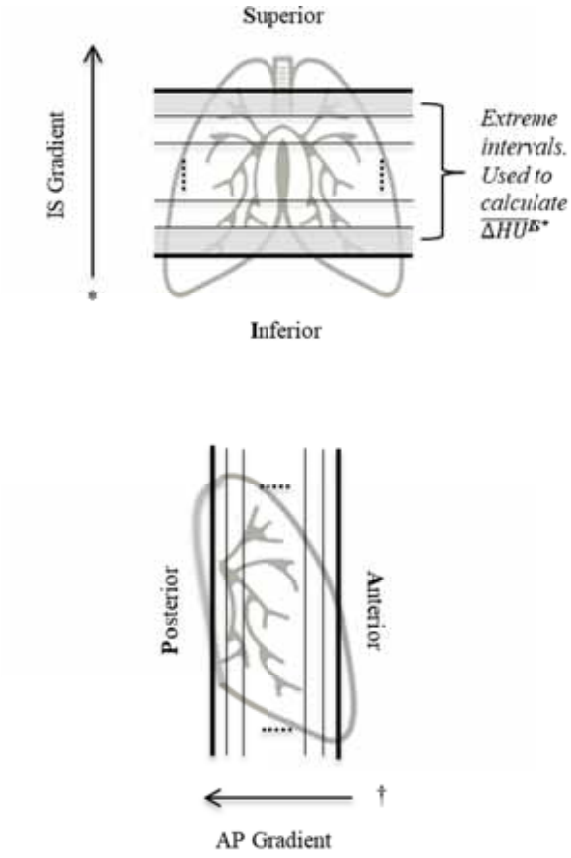

b) Combinatorial features, including inter-lung asymmetry.